Measurements of $^{18}O^{18}O$ and $^{17}O^{18}O$ in the atmosphere and the role of isotope-exchange reactions

Laurence Y. Yeung,[1] Edward D. Young,[1] and Edwin A. Schauble[1]

Received 23 April 2012; revised 24 July 2012; accepted 15 August 2012; published 26 September 2012.

[1] Of the six stable isotopic variants of O_2, only three are measured routinely. Observations of natural variations in $^{16}O^{18}O/^{16}O^{16}O$ and $^{16}O^{17}O/^{16}O^{16}O$ ratios have led to insights in atmospheric, oceanographic, and paleoclimate research. Complementary measurements of the exceedingly rare $^{18}O^{18}O$ and $^{17}O^{18}O$ isotopic variants might therefore broaden our understanding of oxygen cycling. Here we describe a method to measure natural variations in these multiply substituted isotopologues of O_2. Its accuracy is demonstrated by measuring isotopic effects for Knudsen diffusion and O_2 electrolysis in the laboratory that are consistent with theoretical predictions. We then report the first measurements of $^{18}O^{18}O$ and $^{17}O^{18}O$ proportions relative to the stochastic distribution of isotopes (i.e., Δ_{36} and Δ_{35} values, respectively) in tropospheric air. Measured enrichments in $^{18}O^{18}O$ and $^{17}O^{18}O$ yield $\Delta_{36} = 2.05 \pm 0.24‰$ and $\Delta_{35} = 1.4 \pm 0.5‰$ (2σ). Based on the results of our electrolysis experiment, we suggest that autocatalytic $O(^3P)$ + O_2 isotope exchange reactions play an important role in regulating the distribution of $^{18}O^{18}O$ and $^{17}O^{18}O$ in air. We constructed a box model of the atmosphere and biosphere that includes the effects of these isotope exchange reactions, and we find that the biosphere exerts only a minor influence on atmospheric Δ_{36} and Δ_{35} values. $O(^3P)$ + O_2 isotope exchange in the stratosphere and troposphere is therefore expected to govern atmospheric Δ_{36} and Δ_{35} values on decadal timescales. These results suggest that the 'clumped' isotopic composition of atmospheric O_2 in ice core records is sensitive to past variations in atmospheric dynamics and free-radical chemistry.

Citation: Yeung, L. Y., E. D. Young, and E. A. Schauble (2012), Measurements of $^{18}O^{18}O$ and $^{17}O^{18}O$ in the atmosphere and the role of isotope-exchange reactions, *J. Geophys. Res.*, *117*, D18306, doi:10.1029/2012JD017992.

1. Introduction

[2] The global budget of atmospheric O_2 is governed on millennial timescales by the biosphere: O_2 is produced by photosynthesis and consumed primarily by respiration. Glacial-interglacial fluctuations in its bulk isotopic composition (i.e., its $^{18}O/^{16}O$ and $^{17}O/^{16}O$ ratios) over the last 800,000 years are associated with hydrosphere-biosphere feedbacks such as changes in ice sheet volume, evapotranspiration, and primary productivity integrated over ~1,200-year periods [*Bender et al.*, 1994; *Keeling*, 1995; *Blunier et al.*, 2002; *Hoffmann et al.*, 2004; *Severinghaus et al.*, 2009; *Landais et al.*, 2010; *Luz and Barkan*, 2011]. Stratospheric photochemistry also influences the bulk isotopic composition of O_2 by transferring heavy isotopes of oxygen into CO_2; those heavy oxygen isotopes are eventually sequestered in the hydrosphere [*Yung et al.*, 1991; *Thiemens et al.*, 1995; *Yung et al.*, 1997; *Luz et al.*, 1999]. Records of only three O_2 isotopic variants, however, are not sufficient to deconvolve these and other feedbacks.

[3] Measurements of $^{18}O^{18}O$ and $^{17}O^{18}O$ in atmospheric O_2 could offer independent isotopic constraints on O_2 budgets. For instance, the isotopic signature of atmosphere-biosphere interactions could potentially be resolved from that of the hydrosphere because the tendency for ^{18}O-^{18}O and ^{17}O-^{18}O bonds to form upon photosynthesis should be insensitive to the isotopic composition of the source water. Water has no O-O bonds to pass on, so photosynthetic chemistry alone should determine the extent to which ^{18}O and ^{17}O 'clump' together during photosynthesis. In addition, the mass dependence of respiration for $^{18}O^{18}O$ and $^{17}O^{18}O$ could be used in concert with well-known mass dependences for $^{16}O^{18}O$ and $^{16}O^{17}O$ with $^{16}O^{16}O$ to understand oxygen consumption mechanisms in terrestrial and marine environments.

[4] While $^{18}O^{18}O$ and $^{17}O^{18}O$ are exceedingly rare (4 ppm and 1.6 ppm, respectively, in O_2; see Table 1), recent advances in gas-source mass spectrometry suggest that their variations can be measured with "normal" (i.e., low-resolution) isotope-ratio mass spectrometers (IRMS). The routine analysis of rare 'clumped' isotopic variants of CO_2 to high precision (i.e., ≤0.02‰ in $^{16}O^{13}C^{18}O$, which is 46 ppm in CO_2 [*Eiler and Schauble*, 2004; *Eiler*, 2007; *Huntington et al.*,

[1]Department of Earth and Space Sciences, University of California, Los Angeles, California, USA.

Corresponding author: L. Y. Yeung, Department of Earth and Space Sciences, University of California, Los Angeles, CA 90095, USA. (lyyeung@ucla.edu)

0148-0227/12/2012JD017992

Table 1. Properties of O_2 Isotopologues in Air

Isotopologue	Mass (amu)	$\alpha_{j-32,effusion}$	Relative Abundance	Atmospheric Abundance
$^{16}O^{16}O$	31.989829	1	1	0.2095
$^{16}O^{17}O$	32.994046	0.98466	7.8×10^{-4}	1.6×10^{-5}
$^{16}O^{18}O$	33.994076	0.97007	4.1×10^{-3}	8.6×10^{-4}
$^{17}O^{17}O$	33.998263	0.97001	1.5×10^{-7}	3.2×10^{-8}
$^{17}O^{18}O$	34.998293	0.95605	1.6×10^{-6}	3.4×10^{-7}
$^{18}O^{18}O$	35.998322	0.94268	4.2×10^{-6}	8.8×10^{-7}

2009; *Eiler*, 2011]) suggests that variations in $^{18}O^{18}O$ and $^{17}O^{18}O$ could be measured with a precision of order ±0.1‰ using existing technology. The presence of ^{36}Ar in air at 37 times the natural abundance of $^{18}O^{18}O$ (also at mass 36), however, poses a significant analytical challenge for low-mass-resolution instruments.

[5] Here we describe a method to measure natural variations in $^{18}O^{18}O$ and $^{17}O^{18}O$ and we report the first measurements of $^{18}O^{18}O$ and $^{17}O^{18}O$ in tropospheric air. These analyses were made possible by (i) an apparatus for quantitative separation of O_2 from Ar in large samples, (ii) the development of a standardization method based on the reversible decomposition of BaO_2, and (iii) characterization of the extent of isotopic reordering during sample preparation. We demonstrate the accuracy of our methods with two sets of laboratory experiments in which O_2 is subjected to either Knudsen diffusion or electrolysis. The results of those experiments are consistent with theoretical predictions. Last, we report the proportions of $^{18}O^{18}O$ and $^{17}O^{18}O$ in tropospheric air with a 1σ precision of ±0.1‰ and ±0.2‰, respectively, and interpret these results using a box model of the atmosphere.

2. Clumped-Isotope Systematics of O_2

2.1. Notation

[6] $^{18}O^{18}O$ and $^{17}O^{18}O$ distributions are reported against the stochastic (random) distribution of isotopes as defined by the following relationships:

$$^{33}R_{stochastic} = \frac{[^{16}O^{17}O] + [^{17}O^{16}O]}{[^{16}O^{16}O]} = 2\frac{[^{17}O]}{[^{16}O]} = 2\,^{17}R \quad (1a)$$

$$^{34}R_{stochastic} = 2\frac{[^{18}O]}{[^{16}O]} + \frac{[^{17}O][^{17}O]}{[^{16}O][^{16}O]} = 2\,^{18}R + (^{17}R)^2 \quad (1b)$$

$$^{35}R_{stochastic} = 2\frac{[^{18}O][^{17}O]}{[^{16}O][^{16}O]} = 2\,^{18}R\,^{17}R \quad (1c)$$

$$^{36}R_{stochastic} = \frac{[^{18}O][^{18}O]}{[^{16}O][^{16}O]} = (^{18}R)^2 \quad (1d)$$

$$\Delta_{35} = \left(\frac{^{35}R_{measured}}{^{35}R_{stochastic}} - 1\right) \quad (2a)$$

$$\Delta_{36} = \left(\frac{^{36}R_{measured}}{^{36}R_{stochastic}} - 1\right) \quad (2b)$$

in accordance with the recent recommendations by *Coplen* [2011] and conventions for reporting 'clumped' isotope distributions [*Huntington et al.*, 2009; *Dennis et al.*, 2011]. Enrichments and deficits in Δ_n-notation, reported in per mil (‰), reflect proportional deviations from a canonical relationship derived from the bulk isotopic composition, similar to the way in which $\Delta^{17}O$ or $^{17}\Delta$ values are derived from $\delta^{18}O$ and $\delta^{17}O$ values [*Miller*, 2002; *Young et al.*, 2002]. In this case, the canonical relationship is the random occurrence of isotopes in a molecular species.

[7] Conceptually, Δ_n quantifies the abundances of rare isotopic variants relative to those predicted by chance for a given collection of stable isotopes: $\Delta_n = 0$ represents the random distribution of isotopes, whereas a nonzero Δ_n value represents on over- or under-abundance of the indicated rare isotopologue relative to the random distribution. In many instances, this over- or under-abundance of rare isotopologues can be thought of as an excess or deficit in bond ordering, i.e., the tendency of two (or more) rare isotopes to occur as neighbors on the same bond. This definition of Δ_n as an ordering parameter can be misleading, however, when variations in Δ_n occur not through intramolecular bond scission or synthesis, but rather by fractionation of isotopologues. In the latter case, bond ordering is unchanged, but the expected stochastic distribution (e.g., $^{36}R_{stochastic}$) is altered by changing the overall (bulk) isotopic composition of the ensemble (e.g., ^{18}R) [*Eiler*, 2007].

[8] In effect, Δ_n can change either by altering bond ordering in molecules or by altering the reference stochastic composition. The Δ_n values so defined are not conserved quantities precisely because the stochastic distribution changes with bulk isotopic composition. Apparent isotopic bond ordering can therefore be modified by both bond-altering processes and bond-preserving processes. Atmospheric budgets are affected by mechanisms that fall into both categories [*Affek and Eiler*, 2006; *Affek et al.*, 2007; *Yeung et al.*, 2009], so we will discuss the isotopic systematics of O_2 separately in each context.

2.2. Bond-Ordering Equilibrium: Breaking and Making Bonds, but Preserving Atomic Abundances

[9] The familiar carbonate clumped-isotope paleothermometer [*Eiler*, 2011] relies on the change in isotopic bond ordering resulting from a bond-breaking/bond-making process: carbonate mineral growth at equilibrium. In that case, intraphase isotope-exchange equilibrium, when achieved [*Wang et al.*, 2004; *Ghosh et al.*, 2006; *Eagle et al.*, 2010], results in a bond-ordering signature that is independent of the isotopic mass balance between the carbonate and its source water. Bond ordering in the carbonate mineral system, consequently, would then depend only on the temperature of equilibration, and thus would be independent of bulk isotopic composition. These equilibrium bond-ordering values are typically enrichments of up to one per mil in Δ_n because heavy isotopes usually prefer to bond with each other at low temperatures [*Wang et al.*, 2004].

[10] The relevant intraspecies isotopic equilibrium state for O_2 in the atmosphere is gas-phase $O_2 + O_2$ isotope-exchange equilibrium wherein the bulk isotopic composition (and therefore the stochastic distribution) is constant. Bond re-ordering during isotope exchange leads only to changes in Δ_{36} and Δ_{35} values. Theoretical equilibrium Δ_{36} and Δ_{35}

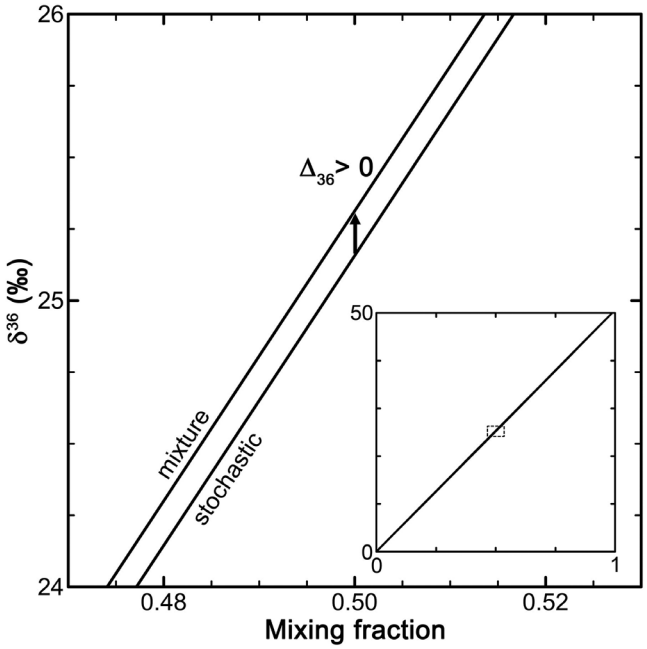

Figure 1. $\Delta_{36} > 0$ anomaly generated by end-member O_2 mixing (mixture of $\delta^{18}O = 25‰$ gas in $\delta^{18}O = 0$ gas, each with initial $\Delta_{36} = 0$). Inset shows the full range of δ^{36}; a 50–50 mixture generates $\Delta_{36} = +0.15$.

values are 1.5–3.0‰ for Δ_{36} and 0.8–1.6‰ for Δ_{35}, between 300 and 200 K [*Wang et al.*, 2004]. Thus, any process that breaks and re-forms O-O bonds without consuming or producing O_2 could, in principle, drive Δ_{36} and Δ_{35} toward equilibrium values with no measurable change in $\delta^{18}O$ and $\delta^{17}O$. Possible mechanisms resulting in equilibration include the reversible decomposition of alkali-earth peroxides (Section 3.2), catalytic isotope exchange on zeolites (Section 3.3) [*Starokon et al.*, 2011], and gas-phase O (^3P) + O_2 isotope exchange reactions (Section 4.2) [*Kaye and Strobel*, 1983].

2.3. Physical Fractionation: Preserving O-O Bonds

[11] The simplest bond-preserving process relevant to the atmosphere is two-component mixing. The isotopic composition (e.g., ^{18}R and $^{36}R_{measured}$) varies linearly with mixing fraction, yet the stochastic distribution, i.e., $^{36}R_{stochastic} = (^{18}R)^2$, varies nonlinearly with mixing fraction. So, even if a mixture consists of two gases with the same initial Δ_n values, mixing yields Δ_n anomalies; Δ_n is not conserved. Mixing equal parts O_2 with $\delta^{18}O \sim 0$ (e.g., ocean water) and $\delta^{18}O \sim 25‰$ (e.g., atmospheric O_2), both starting with $\Delta_{36} = 0$, yields an anomaly of +0.15‰ in Δ_{36} (see Figure 1). This feature of Δ_n notation has been demonstrated in previous work on CO_2 [*Eiler and Schauble*, 2004]. Only in rare cases, such as when the mixing end-members have the same bulk isotopic composition, are Δ_n values conserved upon mixing. Mixing-based budgets for atmospheric Δ_n values are therefore less straightforward than traditional budgets based solely on bulk isotopic δ-notation.

[12] An intuitive relationship between isotopologue fractionation and Δ_n values for O_2 for bond-preserving processes can be derived from the familiar parlance of mass-dependent isotope effects. Here, we follow the practice of describing fractionation factors α related by mass dependences β [*Young et al.*, 2002]:

$$\alpha_{m_i} = \left(\alpha_{m_j}\right)^{\beta_{m_j/m_i}} \tag{3}$$

where the numerical subscripts describe fractionation factors between different O_2 isotopologues of mass m_i and m_j and $^{16}O^{16}O$ ($m = 31.989829$). In equation (3), a fractionation that preserves Δ_{36} and Δ_{35} has mass dependences of $\beta_{36/34} = 0.500$ and $\beta_{35/34} \approx 0.66$, respectively. While $\beta_{36/34} = 0.500$ preserves Δ_{36} as a natural consequence of its definition, $\beta_{35/34}$ values that preserve Δ_{35} vary somewhat with $\beta_{34/33}$ due to the presence of two different rare stable isotopes in $^{17}O^{18}O$. We derive these relationships in Appendix A. Graphically, Δ_n values are approximated by horizontal excursions on a triple-isotopologue plot relative to the mass-dependent relationship for the stochastic distribution, i.e., δ^{36} excursions relative to a $\beta_{36/34} = 0.500$ line on a δ^{34} versus δ^{36} plot (see Figure 2). Examples of these mass dependences can be found in gravitational fractionation and Knudsen diffusion.

[13] A stagnant air column in a gravitational potential will have a higher partial pressure of heavy isotopologues at the base. This fractionation depends on mass according to the barometric formula. For a species of mass m, its partial pressure P at a height Z and temperature T can be related to the surface partial pressure P_0 by the equation:

$$\frac{P}{P_0} = e^{m\frac{gZ}{R_G T}} \tag{4}$$

where g is the acceleration due to gravity (9.81 m s^{-2}) and R_G is the gas constant. This equation can be recast to reflect isotopic ratios:

$$\alpha_{m_i,gravitation} = \frac{^{m_i}R_{height}}{^{m_i}R_{surface}} = e^{(m_i - m_{32})\frac{gZ}{R_G T}} \tag{5}$$

where m_{32} is the mass of $^{16}O^{16}O$. One can now recognize that because the mass difference between $^{16}O^{18}O$ and $^{16}O^{16}O$, $(m_{34} - m_{32})$, is exactly half the mass difference between $^{18}O^{18}O$ and $^{16}O^{16}O$, $(m_{36} - m_{32})$, we have $(\alpha_{34})^2 = \alpha_{36}$. Therefore, $\alpha_{34} = (\alpha_{36})^{0.5}$, or $\beta_{36/34} = 0.5$, and gravitational fractionation has a negligible effect on Δ_{36} (even when including the contribution from $^{17}O^{17}O$; see Appendix A). A similar argument can be made to show that $\beta_{35/34} = 0.666$, resulting in no fractionation for Δ_{35}. This behavior for Δ_{36} and Δ_{35} is distinct from the bulk-isotope fractionations of 0.1–1‰ in natural systems [*Craig et al.*, 1988; *Severinghaus et al.*, 1996].

[14] Knudsen diffusion, in contrast, leads to changes in both Δ_{36} and Δ_{35}. Graham's law of effusion states that the flux of gas through an orifice smaller than the mean free path of that gas will be inversely proportional to the square root of its mass. For pure O_2 gas, the isotopic fractionation factor is:

$$\alpha_{m_i - m_{32},effusion} = \frac{^{m_i}R_{diffused}}{^{m_i}R_{initial}} = \sqrt{\frac{m_{32}}{m_i}}. \tag{6}$$

Mass dependences for effusion can be derived from these α values to be $\beta_{36/34} = 0.515$ and $\beta_{35/34} = 0.676$ (see Table 1),

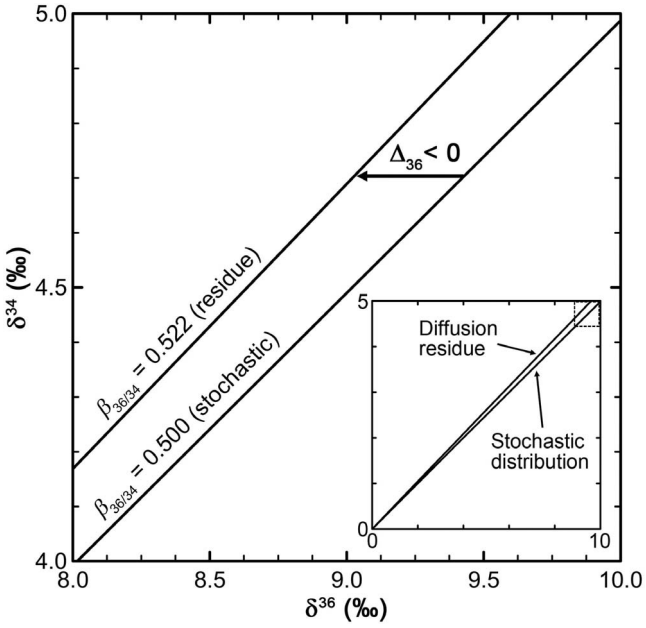

Figure 2. Example of a bond-preserving fractionation process that can generate Δ_{36} anomalies. Knudsen diffusion subject to Rayleigh fractionation has $\beta_{36/34} = 0.522$ in the residue, which generates a $\Delta_{36} < 0$ anomaly relative to the stochastic distribution ($\beta_{36/34} = 0.500$). The arrow depicts an anomaly of $\Delta_{36} = 0.4‰$.

which lead to Δ_{36} and Δ_{35} increases in the isotopically lighter diffused population: O_2 that has leaked through a critical orifice from an infinite reservoir is lower in $\delta^{18}O$ and $\delta^{17}O$ by 29.9‰ and 15.3‰, respectively, but higher in Δ_{36} and Δ_{35} by 1.7‰ and 0.9‰, respectively, than the reservoir. This fractionation is a classic example of 'clumped' isotope signatures changing due to shifts in the stochastic reference frame (i.e., the bulk isotopic composition of the gas).

[15] In a finite system, the residue population will be fractionated in the opposite direction: Higher in $\delta^{18}O$ and $\delta^{17}O$, but lower in Δ_{36} and Δ_{35} (see Figure 2). Furthermore, this closed system has β values that are slightly larger than those of the infinite system due to the effective α values derived from Rayleigh fractionation relationships:

$$R_{residue} = R_{initial} f^{\alpha_{effusion}-1} \quad (7)$$

$$R_{diffused} = R_{initial} \frac{1 - f^{\alpha_{effusion}}}{1 - f} \quad (8)$$

where f represents the fraction of the initial gas remaining, and α for the Rayleigh system is defined by $R_{diffused}/R_{initial}$ [*Young et al.*, 2002]. $\beta_{36/34}$ and $\beta_{35/34}$ values, defined by connecting the $R_{diffused}$ and $R_{residue}$ corresponding to a single f value, range from 0.515–0.522 and 0.676–0.681, respectively, depending on f. We explore these particular systematics experimentally in Section 4.1.

3. Methods

[16] To analyze $^{18}O^{18}O$ and $^{17}O^{18}O$ in O_2, argon was first removed from samples using gas chromatography at sub-ambient temperatures. Next, the purified O_2 was analyzed against a working reference gas on an IRMS, where the residual Ar content was also measured (as a $m/z = 40$ voltage ratio). Then, standard gases with similar bulk isotopic composition, but a 'clumped-isotope' composition near the stochastic distribution, were prepared and analyzed over a range of Ar concentrations. Reported Δ_{36} and Δ_{35} values correspond to the excesses or deficits in $^{18}O^{18}O/^{16}O^{16}O$ and $^{17}O^{18}O/^{16}O^{16}O$ ratios relative to the stochastic distribution of isotopes after correction for the residual Ar signals and deviations from a purely stochastic distribution in the reference gases (see Appendix B).

3.1. Sample Handling and Purification

[17] O_2 samples (150–200 μmol O_2) were transferred to and from a gas chromatographic system through two glass U-traps at −196°C on a high-vacuum glass line pumped by a diaphragm-backed turbomolecular pump (Pfeiffer HiCube), which had a typical baseline pressure of $\sim 5 \times 10^{-6}$ mbar. Purified O_2 samples were adsorbed for 10 min onto small glass fingers filled with molecular sieve 5A pellets at −196°C before analysis on the IRMS.

[18] The gas chromatographic (GC) system, which was designed to separate O_2 from Ar and N_2, consisted of a reconditioned HP 5890 Series II GC capable of cryogenic cooling with liquid nitrogen and thermal conductivity detection. First, samples were adsorbed onto degassed silica gel pellets in a U-trap at −196°C for ~30 min. The U-trap was then immersed in warm water (~60°C) while an ultra-high-purity helium carrier gas (>99.9995%; Grade 5.5) flowed through it to desorb the sample. The desorbed sample was then injected onto the GC column (3 m, molecular sieve 5A, 80/100 mesh; Restek) using two 4-way VICI/Valco switching valves. As an additional precaution against atmospheric leaks, the switching valves were isolated in He-flushed "jackets." The eluent from the GC column was collected on a second silica gel U-trap downstream from the GC column at −196°C. Air samples were passed through the GC system a second time to remove residual Ar remaining from the first pass. A diagram of the vacuum/GC extraction and purification system is shown in Figure 3.

[19] Baseline separation of Ar, O_2, and N_2 was achieved at T ≤ −65°C, and routine separations were carried out at −80°C. The volumetric flow rate was 25 mL min^{-1} (~23 psi He carrier). Argon typically eluted near 30 min, while O_2 eluted near 38 min (see Figure 3); collection of O_2 lasted 23–25 min, starting near minute 37. After collection of O_2, the column temperature was raised to 200°C and the He pressure was raised to 40 psi to elute N_2.

[20] The conditions for O_2/Ar separation were chosen to minimize both residual Ar and total sample preparation time. Higher O_2/Ar elution temperatures decreased the O_2/Ar peak resolution and also increased the amount of Ar in the purified product. For instance, raising the temperature to 25°C after the Ar peak eluted, which reduced the O_2 collection time to ~15 min, actually *increased* the Ar content relative to a 25-min collection at −80°C. Furthermore, using a 6-m molecular sieve 5A column yielded no improvements in O_2/Ar separation efficiency due to on-column dispersion and a longer O_2 collection time. However, installing a U-trap to purify the helium carrier filled with molecular sieve 5A and

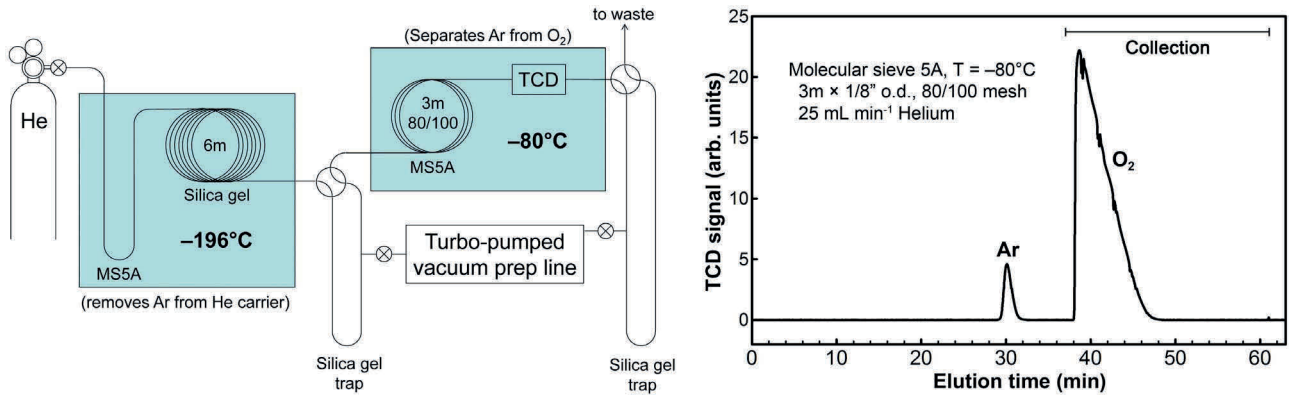

Figure 3. Schematic of the GC and vacuum-line extraction and purification system. During sample purification, helium flows through both silica gel traps. After GC separation, the switching valves are rotated to isolate the vacuum prep line from the helium flow. Also shown is a typical gas chromatogram of O_2/Ar separation for ~20 cm^3 samples of air. N_2 was eluted from the column at higher temperatures after collection of O_2.

a 6-ft silica gel column (45–60 mesh; SRI International), both at −196°C, resulted in a twofold improvement in Ar removal. Consequently, we believe that Ar impurities in the helium stream ultimately limited O_2 purity in the current system. Typical air preparations with two passes through our system resulted in 1–5 ppm ^{40}Ar (i.e., 3–17 ppb ^{36}Ar) in O_2. Additional small ion corrections at $m/z = 36$ were necessary for high-precision measurements of $^{18}O^{18}O$ (see Appendix B).

3.2. Standardization

[21] The use of a stochastic reference frame for O_2 isotopologue abundances requires that one develop methods to generate laboratory standards with known Δ_{36} and Δ_{35} values over a range of bulk isotopic composition [*Huntington et al.*, 2009; *Dennis et al.*, 2011]. High-temperature standards, reflecting $\Delta_{36} \sim \Delta_{35} \sim 0$, are a convenient reference close to the stochastic distribution. We utilized the reversible decomposition of BaO_2 to generate Ar-free O_2 at high-temperature isotopic equilibrium:

$$2BaO_{2(s)} \rightleftharpoons 2BaO_{(s)} + O_{2(g)} \quad (9)$$

Argon can be pumped out at low temperatures so O_2 will evolve exclusively from the lattice when the peroxide is heated above 600°C [*Tribelhorn and Brown*, 1995]. The oxygen atoms in each product O_2 molecule originate from different peroxide groups in the mineral lattice [*Tribelhorn and Brown*, 1995], and the process is reversible, so BaO_2 decomposition at high temperatures should produce a 'clumped-isotope' distribution in the evolved O_2 reflecting high-temperature equilibrium; experimental studies indicate that equilibrium can be maintained at T < 1000°C at low heating/cooling rates [*Tribelhorn and Brown*, 1995; *Jorda and Jondo*, 2001]. This method is general to alkali-earth peroxides, and is similar to that used by *Asprey* [1976] to synthesize pure F_2 gas from the reversible decomposition of solid $K_2NiF_6{\cdot}KF$, i.e., $2(K_2NiF_6{\cdot}KF)_{solid} \rightleftharpoons 2(K_3NiF_6)_{solid} + F_2$.

[22] To estimate the clumped-isotope composition of O_2 derived from BaO_2 decomposition, theoretical models for bond-ordering in O_2 and BaO_2 were used. A comparative model of isotopologue ordering in O_2 was calculated using the same method and data as *Wang et al.* [2004], using the harmonic frequency of $^{16}O^{16}O$ [*Huber and Herzberg*, 1979]. Vibrational frequencies of isotopologues were determined from their reduced masses, and the resulting estimate was essentially identical to the harmonic model of *Wang et al.* [2004]. We note that *Wang et al.* [2004] showed that inclusion of anharmonic terms has a minor effect on ordering equilibria for O_2, <0.01‰ at room temperature.

[23] BaO_2 is predicted to be much less enriched in multiply substituted isotopologues than O_2 is at all temperatures (see Figure 4 and Appendix C). It is also predicted to have lower $^{18}O/^{16}O$ and $^{17}O/^{16}O$ ratios. Above 600°C, Δ_{36} and Δ_{35} are both predicted to be <0.01‰ in BaO_2, whereas they

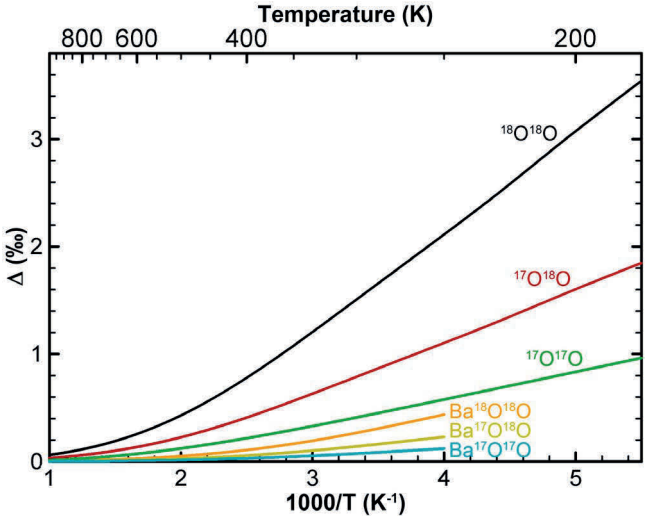

Figure 4. Calculated 'clumped' isotopic fractionation for the BaO_2 and O_2 systems relative to atomic O vapor.

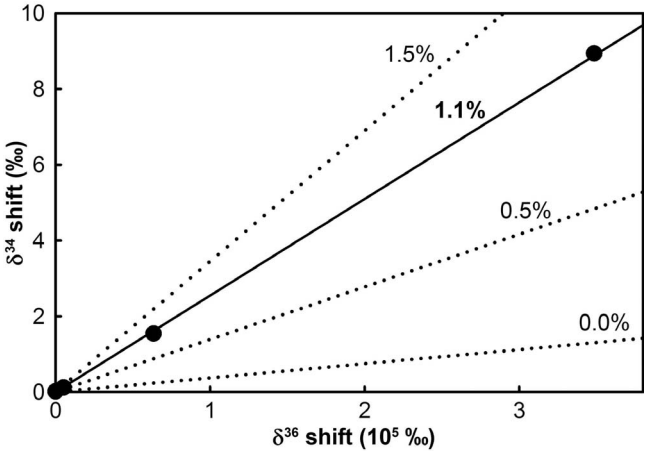

Figure 5. Extent of ^{18}O isotope exchange in the IRMS ion source, measured by the method of standard additions on a $^{18}O^{18}O$-spiked sample of O_2. The initial $^{18}O^{18}O$ "spike" yielded a mixture with $\delta^{36} \sim 3.4 \times 10^5$ ‰, and the isotopic composition of the standard is represented by $\delta^{34} = \delta^{36} = 0$. Solid line depicts the standard-additions curve consistent with the laboratory data (1.1% isotopic reordering in the ion source). The dotted lines are standard-additions curves for different amounts of isotopic reordering in the ion source that demonstrate the sensitivity of the method.

are predicted to be ≤0.08‰ in O_2. As with the C-O bonding system, there appears to be a strong correlation between equilibrium constants and bond order, with double-bonded species (e.g., CO_2 and O_2) showing larger enrichments in multiply substituted isotopologues than species with lower-order bonds (e.g., C–O bonds in carbonate and bicarbonate and O–O bonds in peroxide) [*Wang et al.*, 2004; *Schauble et al.*, 2006; *Eagle et al.*, 2010].

[24] To decompose BaO_2 in the laboratory, BaO_2 powder was first loaded into 1/4″ OD quartz tubes and pumped to 10^{-6}–10^{-5} mbar overnight. Afterwards, the quartz tubes were sealed with a torch and placed in a tube furnace at 800°C for 2.5 h (calculated $\Delta_{36} = 0.03$‰ and $\Delta_{35} = 0.02$‰). Hot breakseals were quenched immediately when plunged into cold water. As a test of the breakseal method, we also performed experiments in which BaO_2 was heated to 800°C for 2.5 h in an evacuated 9-mm ID quartz-and-glass tube that extended from the interior of the tube furnace to an aliquot volume. In this arrangement, the evolved O_2 was allowed to equilibrate with BaO and BaO_2 only at high temperatures, unlike the breakseal-quenching process, in which some low-temperature isotope exchange might be present. We did not observe significant differences beyond typical experimental scatter in the resulting Δ_{36} and Δ_{35} values measured (±0.1–0.3‰, depending on the isotopologue), consistent with the breakseal method yielding O_2 at high-temperature equilibrium.

[25] A second method for generating high-temperature O_2 standards in breakseals was also developed. In that method, O_2 was collected into breakseals with molecular sieve 5A and Platinum wire and heated to 1000°C (expected $\Delta_{36} = 0.02$‰ and $\Delta_{35} = 0.01$‰). Hot breakseals were again quenched immediately by plunging them into cold water. While we cannot rule out a lower 'blocking' temperature for gases prepared in this manner, high O_2 concentrations should passivate platinum when $T < 500$°C [*Brewer*, 1953], where $\Delta_{36} = 0.11$‰ and $\Delta_{35} = 0.06$‰, so O_2 standards prepared in this manner are still expected to be near the stochastic distribution, and nearly indistinguishable from it within the analytical uncertainty. We note that this method altered the bulk isotopic composition of O_2, probably by isotopic exchange with the molecular sieve and/or quartz, but the bulk isotopic fractionation was relatively consistent.

3.3. Other Sources of Isotopic Reordering

[26] While the oxygen-oxygen bond in O_2 is not easily broken (bond dissociation enthalpy 118 kcal mol^{-1}), any isotopic reordering during sample preparation and analysis will result in an alteration of Δ_{36} and Δ_{35}. Thus, we performed experiments with O_2 samples enriched in $^{18}O^{18}O$ to quantify the extent of isotopic reordering in our sample preparation scheme.

[27] The extent of isotopic reordering in the source of the IRMS was determined by measuring the isotopic composition of our O_2 standard gas "spiked" with an aliquot of ≥97% $^{18}O^{18}O$ (Cambridge Isotope Labs). Significant isotopic reordering in the IRMS source would result in a significant increase in δ^{34} (500–600‰ for our $^{18}O^{18}O$ spike size), with little change in δ^{36} relative to the unspiked O_2, due to fragmentation-recombination reactions such as

$$^{16}O^{16}O + e^- \rightarrow {}^{16}O^+ + {}^{16}O^{2-} \quad (10)$$

$$^{18}O^{18}O + {}^{16}O^+ \rightarrow {}^{16}O^{18}O + {}^{18}O^+. \quad (11)$$

Zero isotopic reordering would yield (i) no change in $\delta^{18}O$ beyond any $^{16}O^{18}O$ present in the ≥97% $^{18}O^{18}O$ gas and (ii) a large change in the $m/z = 36$ voltage. In our experiment, we observed only a small change in δ^{34} (∼9‰) and a relatively large change in δ^{36} (3.4×10^5‰), indicating that the extent of O_2 isotopic reordering in the IRMS source was small. We further quantified the extent of isotopic reordering in the IRMS source by the method of standard additions (see Figure 5). The results were consistent with only 1% of the bonds being reordered toward an (probably high-temperature) isotope-exchange equilibrium in the IRMS source.

[28] Similar $^{18}O^{18}O$ spike-reordering tests were performed with molecular sieve adsorbents because O_2 can exchange isotopes with the molecular sieves and/or reorder its isotopes on the surface of molecular-sieve zeolites at low temperatures [*Starokon et al.*, 2011]. Adsorption of O_2 onto the molecular sieve 5A at −196°C, followed by desorption at 240°C for 30 min, resulted in ∼1% isotopic reordering. Passing gas through the GC system only reordered isotopes in O_2 after the column was baked with a helium flow at 350°C overnight (∼12h). In that case, the bond ordering resembled equilibrium at the GC temperature, −80°C. During a typical air preparation, O_2 was exposed to molecular sieve four times (twice through the GC and twice in a sample finger), which would result in a reduction in Δ_{36} signal magnitude of ∼4% (i.e., ∼0.08‰ for $\Delta_{36} = 2$‰) We observed some evidence for isotopic reordering (2–3%) upon exposure to a pressure gauge that had both Pirani-type and inverted magnetron

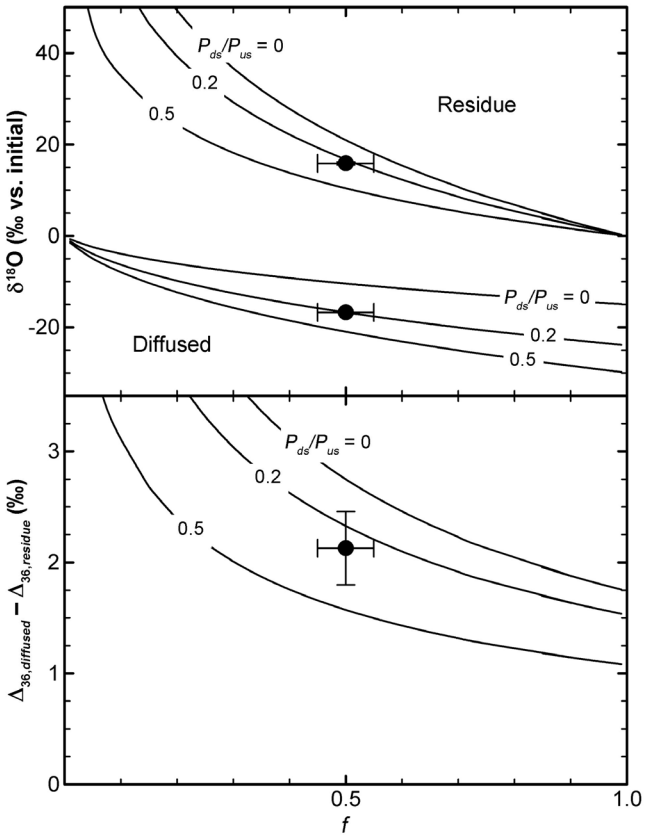

Figure 6. Theoretical and experimental isotopic fractionation in (top) $\delta^{18}O$ and (bottom) Δ_{36} due to Knudsen diffusion. Differing amounts of back-diffusion (i.e., P_{ds}/P_{us}) yield different fractionations. Experimental points are shown with estimated 1σ measurement uncertainties.

capabilities (Edwards WRG-S; perhaps due to the tungsten electrode exposed to vacuum), so we isolated the gauge from O_2 during our sample preparation.

4. Experiments

4.1. Knudsen Diffusion: Mass Fractionation While Preserving O-O Bonds

[29] We performed experiments to induce shifts in Δ_{36} and Δ_{35} by Knudsen diffusion of O_2. These experiments provide a useful test of our analytical methods because the changes in Δ_{36} and Δ_{35} due to diffusion are readily calculable. We showed, in Section 2.3, that fractionation factors α for O_2 diffusion through a critical orifice lead to measured effective $\beta_{36/34}$ and $\beta_{35/34}$ values of between 0.515–0.522 and 0.676–0.681, respectively, for a system subject to Rayleigh fractionation. In a laboratory setting, back-diffusion through the critical orifice can also alter effective α and β values: Because the "downstream" volume is never ideal (finite size and pressure), gas can travel "upstream" into the high-pressure volume. This back-diffusion is subject to the same isotopic fractionation described in equations (6)–(8), but with a time-dependent $R_{initial}$ value corresponding to the changing $R_{diffused}$ in a Rayleigh system; Benedict showed that the resulting fractionation factors could be described by the equation [*Benedict*, 1947; *Naylor and Backer*, 1955]:

$$\alpha_{m_i-m_{32}} - 1 = \left(\sqrt{\frac{m_{32}}{m_i}} - 1\right)\left(1 - \frac{P_{ds}}{P_{us}}\right) \qquad (12)$$

where P_{ds}/P_{us} is the ratio of pressures in the downstream and upstream volumes.

[30] Assuming no back diffusion, i.e., P_{ds}/P_{us} = 0, and f = 0.5, the difference in $\delta^{18}O$, $\delta^{17}O$, Δ_{36} and Δ_{35} between the diffused and residue populations is calculated to be −41.9‰, −21.4‰, +2.7‰, and +1.4‰ respectively. For P_{ds}/P_{us} = 0.1 and f = 0.5, the difference between the diffused and residue populations is calculated to be −37.7‰, −19.2‰, +2.5‰, and +1.3‰, respectively. Because the mass dependence of diffusion governs both forward and back-diffusion, $\beta_{36/34}$ and $\beta_{35/34}$ values do not change appreciably for f = 0.5 (i.e., $\beta_{36/34}$ = 0.5170 versus 0.5174 for P_{ds}/P_{us} = 0 versus 0.1, respectively). Thus, back-diffusion mainly reduces the bulk isotopic fractionation relative to the unidirectional Rayleigh limit.

[31] In our pinhole diffusion experiment, we allowed O_2 gas to diffuse from a 5-L glass bulb through an orifice of known diameter into a vacuum. We measured the isotopic composition of both the diffused and residue populations. The initial pressure in the 5-L bulb was 1.0 mbar, resulting in a mean free path, λ, of 100 μm. Molecular oxygen diffused through a laser-drilled orifice (Lenox Laser) with a diameter, D, of 75 ± 7.5 μm. It then passed through a length of flexible bellows tubing and a second 5-L bulb and two U-traps at −196°C (total volume ~5.1 L) before being collected onto a silica gel trap at −196°C for purification on the GC system. The purpose of the second 5-L bulb was to reduce back-diffusion through the critical orifice, as adsorption of O_2 onto silica gel is a slow process. The steady state pressure on the "diffused" side of the apparatus was $\leq 10^{-1}$ mbar during the experiment. After 3 h of diffusion, both bulbs were isolated from the critical orifice, and the diffused population was allowed to adsorb onto the silica gel trap for another 60 min. Both the diffused and residue population were analyzed on the IRMS.

[32] The results of the diffusion experiment are shown in Figure 6 and Table 2. As predicted for a diffusion-limited system, the diffused gas exhibited decreases in $\delta^{18}O$ and $\delta^{17}O$ and increases in Δ_{35} and Δ_{36}. In addition, using equation (12) with P_{ds}/P_{us} = 0.2 yields good agreement between theory and experiment. The measured isotopic fractionations yield a $\beta_{36/34}$ value of 0.517 ± 0.002 (1σ), consistent with the predicted $\beta_{36/34}$ of 0.518. An assumption of no back-diffusion, i.e., P_{ds}/P_{us} = 0, instead predicts bulk- and clumped-isotope fractionations that are smaller, and an f value that is larger, than the measured values.

[33] Back-diffusion of order 20% is possible given the relatively slow O_2 adsorption rate onto silica gel, which resulted in the relatively high steady state downstream pressure of $\leq 10^{-1}$ mbar. However, the size of our critical orifice (λ/D = 1.33) also yielded gas flow properties in the transition region between purely molecular (Knudsen) and purely viscous (Poiseuille) flows. Because viscous flow does not fractionate isotopologues, while Knudsen diffusion fractionates isotopologues according to Graham's law, a small amount of viscous flow probably reduces Graham's law

Table 2. Results of Knudsen-Diffusion Experiment

	Measured $f = 0.50 \pm 0.05$			Predicted		
	Diffused	Residue	Diffused – Residue	Effusion	$f = 0.591$, Rayleigh	$f = 0.529$, $P_{ds}/P_{us} = 0.2$, Plus Back-Diffusion
$\delta^{18}O$/‰	−16.743	15.870	−32.613	−29.927	−38.788	−32.616
$\delta^{17}O$/‰	−8.549	8.073	−16.622	−15.336	−19.800	−16.651
Δ_{35}/‰	1.0 ± 0.6	-0.3 ± 0.6	1.3 ± 0.7	0.9	1.3	1.2
Δ_{36}/‰	1.39 ± 0.16	-0.74 ± 0.29	2.13 ± 0.33	1.7	2.5	2.3

fractionations with a scaling factor on $(\alpha - 1)$ similar to the effect of back-diffusion in equation (12). Furthermore, theoretical calculations by *Wahlbeck* [1971] suggest that gas flux through the orifice is enhanced by ~20%, presumably due to increasing viscous flow, relative to the flux predicted for purely molecular flow at $\lambda/D = 1.33$. Thus, we are unable to distinguish between back-diffusion and partially viscous flow leading to a 20% reduction in $(\alpha - 1)$ values in this experiment. Decreasing the orifice size to achieve purely molecular flow ($\lambda/D \geq 10$, i.e., $D \leq 10$ μm at 1 mbar) would reduce the mass flow rate through the orifice more than 50-fold, increasing the experiment's duration to about a week. Such timescales are impractical for this experiment because atmospheric leaks would have become important. Cryo-trapping the diffused O_2, however, would eliminate back-diffusion and isolate the viscous-flow contribution to the observed diffusive isotopic fractionation.

4.2. O_2 Electrolysis: Bond-Ordering Equilibration Independent of Bulk Isotopic Composition

[34] $O(^3P) + O_2$ isotope exchange reactions can chemically reorder O-O bonds in O_2. These reactions are part of the Chapman cycle found in the stratosphere [*Mauersberger et al.*, 1999; *Gao and Marcus*, 2001; *Van Wyngarden et al.*, 2007]:

$$Q(^3P) + O_2 \rightarrow OOQ^* \rightarrow O(^3P) + OQ \quad (13a)$$

$$\overset{M}{\rightarrow} OOQ \quad (13b)$$

where Q denotes an isotope of oxygen and M is a third body such as another O_2 molecule. In a closed system, the bulk isotopic composition is determined by the O_2/O_3 mass balance and isotope effects in O_3 formation [*Hathorn and Marcus*, 1999, 2000; *Gao and Marcus*, 2001], while oxygen atoms in their ground electronic state, $O(^3P)$, act as catalysts for bond reordering in molecular oxygen.

[35] When a ground-state oxygen atom forms a bond with an O_2 molecule, it has three possible fates: ozone formation, inelastic scattering, and isotope exchange. A stable ozone molecule forms only when a third body, M, absorbs the excess energy released during O-O bond formation. Without that third body, the metastable O_3 can redissociate to $O(^3P) + O_2$. If the O-O bond that breaks is the one that just formed, then inelastic scattering results. If the other bond breaks, then isotope exchange occurs. In either case, the liberated $O(^3P)$ atom perpetuates an autocatalytic cycle. Consequently, reaction (13a) occurs at rates at least several hundred times faster than that of (13b) at pressures of ~50 mbar [*Kaye and Strobel*, 1983; *Johnston and Thiemens*, 1997; *Wiegell et al.*, 1997]. This difference in rates will decouple Δ_{36} and Δ_{35} values from the bulk isotopic composition of O_2: While $^{36}R_{measured}$ and $^{35}R_{measured}$ change with every applicable isotope-exchange event, $^{36}R_{stochastic}$ and $^{35}R_{stochastic}$ vary only with $\delta^{18}O$ and $\delta^{17}O$, which is governed by the O_2/O_3 mass balance.

[36] Excited atomic oxygen, $O(^1D)$, could also exchange isotopes with O_2, but $O(^3P)$ chemistry should dominate the bond-ordering budget in most systems. Nearly all $O(^1D)$ atoms will be quenched to $O(^3P)$ eventually by N_2 or O_2, after which isotope exchange proceeds autocatalytically. Even in the presence of unconventional chemical physics on the O_3 potential energy surface, the large number of $O(^3P) + O_2$ isotope exchange reactions occurring is predicted to yield an isotopic distribution in O_2 that is controlled by differences in zero-point energies in the O_2 isotopologues [*Hathorn and Marcus*, 1999, 2000; *Gao and Marcus*, 2001]. Δ_{36} and Δ_{35} values, as measures of bond ordering and not bulk isotopic composition, are therefore expected to reflect *mass-dependent* isotopic equilibrium, while $\delta^{18}O$ and $\delta^{17}O$, being measures of bulk isotopic composition only, will reflect the *mass-independent* isotope effects that dominate ozone-formation chemistry.

[37] To realize $O(^3P) + O_2$ isotope exchange in the laboratory, O_2 was electrolyzed with a radio-frequency discharge in a manner similar to the classic experiments of *Heidenreich and Thiemens* [1983]. We fabricated a vessel out of a 100-mL round-bottom flask, a tungsten electrode (1.5 cm exposed to vacuum), and a 9-mm Louwers-Hapert vacuum valve outfitted with fluorinated-elastomer O-rings (Markez). The exterior wire lead was jacketed so the entire vessel could be immersed in a cold bath without wetting the wire. Electrolysis was initiated by setting a Tesla coil at its lowest audible level for one hour. Pressures inside the vessels were 50 to 60 mbar at 25°C, resulting in a mean free path $\lambda \leq 30$ μm versus the vessel's 2-cm radius; under these conditions, $O(^3P) + O_2$ reactions should primarily occur in the gas phase with only a minor contribution from surface chemistry. After the experiment, O_3 was cryogenically separated from O_2, which was passed through the GC system twice to remove residual O_3 and any contaminants.

[38] Electrolysis experiments were performed at three bath temperatures: 25°C, −30°C, and −80°C. The vessel temperature was maintained by submerging the round-bottom flask into a water bath (25°C experiment) or ethanol bath (−30°C and −80°C experiments). Because the Tesla coil added heat to the vessel, the bath temperature was monitored and, if necessary, the bath was cooled, every 10 to 15 min. This procedure yielded stable bath temperatures to within ±3°C. Temperatures inside the reaction vessel were not measured, but we performed several additional blank experiments to

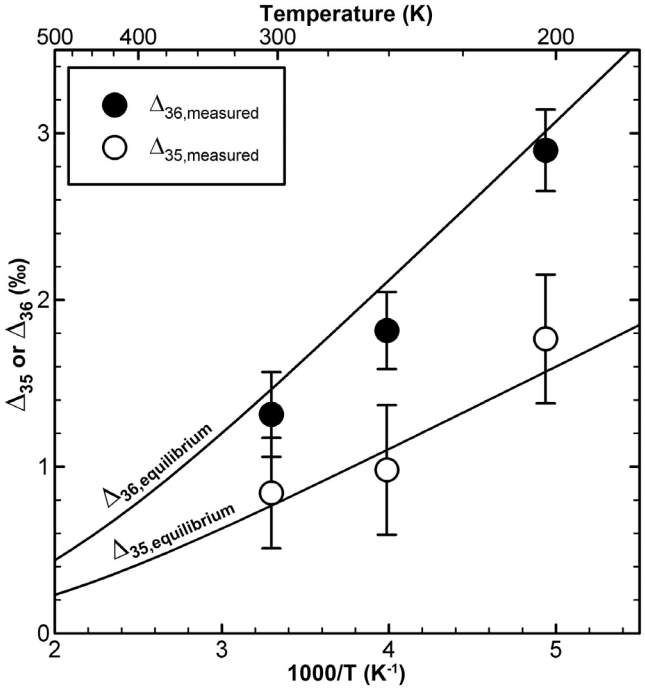

Figure 7. $O + O_2$ isotope exchange rapidly re-orders ^{18}O-^{18}O and ^{17}O-^{18}O bonds in O_2. Electrolysis of pure, stochastically ordered O_2 (i.e., $\Delta_{36} \approx \Delta_{35} \approx 0$) at low temperatures with a RF discharge resets Δ_{36} and Δ_{35} near their equilibrium values. Error bars show analytical 2σ uncertainties.

estimate the effective internal temperatures: A thermocouple was inserted into the reaction vessel while it was open to atmosphere ($P \sim 1$ bar) and the temperature was monitored for 10 min with the Tesla coil on, simulating experimental conditions. Internal temperatures increased monotonically in all cases, by +10°C, +16°C, and +18°C for the 25°C, −30°C, and −80°C baths, respectively. Therefore, we estimate that effective, time-integrated temperatures inside the reaction vessel were +5°C, +8°C, and +9°C warmer than the 25°C, −30°C, and −80°C baths, respectively.

[39] The results of the electrolysis experiments are presented in Figure 7 and Table 3. Δ_{36} and Δ_{35} are consistent with bond-ordering equilibrium at the temperature of the experiments (1 to 3‰). $\delta^{18}O$ and $\delta^{17}O$ were depleted <1‰ along a slope = 1.0 line in triple-isotope space ($\delta^{17}O$ versus $\delta^{18}O$), indicating that <5% of the O_2 was converted into stable O_3 [*Heidenreich and Thiemens*, 1983]. The depletions increased as temperature decreased (faster O_3 formation rate), as expected for a changing O_2/O_3 mass balance. These results are consistent with our prediction that isotopic ordering (Δ_{36} and Δ_{35} values) and bulk-isotope abundances

Table 3. Results of Electrolysis Experiments

	Measured				Predicted	
T/°C	Change in $\delta^{18}O$ (‰)	Change in $\delta^{17}O$ (‰)	Δ_{35}[a] (‰)	Δ_{36}[a] (‰)	Δ_{35} (‰)	Δ_{36} (‰)
−71	−0.920	−0.895	1.8 ± 0.2	2.89 ± 0.12	1.6	3.01
−22	−0.479	−0.452	1.0 ± 0.2	1.81 ± 0.12	1.1	2.11
+30	−0.458	−0.405	0.8 ± 0.2	1.31 ± 0.13	0.8	1.46

[a]Uncertainties correspond to 1σ.

Table 4. Measured Isotopic Composition of O_2 in Tropospheric Air

Sampling Date[a]	$\delta^{18}O$[b] (‰)	$\delta^{17}O$[b] (‰)	Δ_{36} (‰)	Δ_{35} (‰)
10/14/11	23.398	11.912	1.91	1.1
10/19/11	23.477	11.961	2.04	1.6
10/20/11	23.307	11.869	2.14	1.4
10/21/11	23.552	12.003	2.01	1.6
10/24/11	23.388	11.914	2.13	1.4
Average ± 2 s.e.[c]	23.424 ± 0.083	11.932 ± 0.046	2.05 ± 0.08	1.4 ± 0.2

[a]Dates are given as mm/dd/yy.
[b]The $\delta^{18}O$ and $\delta^{17}O$ are reported against VSMOW using a laboratory standard gas calibrated with San Carlos Olivine ($\delta^{18}O$ = 5.2‰, $\delta^{17}O$ = 2.7‰). Our results are consistent with a previous direct determination of the O_2 bulk isotopic composition ($\delta^{18}O$ = 23.51‰ and $\delta^{17}O$ = 12.18‰) [*Thiemens and Meagher*, 1984]. A more recent measurement has reported $\delta^{18}O$ = 23.88‰ and $\delta^{17}O$ = 12.08‰ [*Barkan and Luz*, 2005].
[c]External standard error of replicate gas preparations; systematic uncertainties increase 2σ limits to ±0.24‰ and ±0.5‰ in Δ_{36} and Δ_{35}, respectively.

are controlled by two different mechanisms in this system, one of which [$O(^3P) + O_2$ isotope exchange] equilibrates Δ_{36} and Δ_{35} despite persistent disequilibrium in the O_2/O_3 system.

[40] Autocatalytic $O(^3P) + O_2$ isotope exchange is the most likely mechanism to equilibrate Δ_{36} and Δ_{35} because of (i) its high bimolecular reaction rate, (ii) the paucity of permanent $O(^3P)$ sinks in the experiment, (i.e., surfaces, O_3, or another $O(^3P)$), and (ii) its minimal effects on $\delta^{18}O$ and $\delta^{17}O$ of O_2. Furthermore, we observe nearly quantitative agreement between our measured Δ_{36} and Δ_{35} values and those expected from theory [*Hathorn and Marcus*, 2000; *Wang et al.*, 2004]. Wall/surface effects cannot be ruled out, but the results from a previous study of O_3 chemistry by *Morton et al.* [1990] suggest wall effects are insignificant in our apparatus. For example, the surface of the tungsten electrode during electrolysis likely resembles a high-temperature plasma, so significant oxygen-isotope exchange on that surface would probably reflect high temperatures rather than the low temperatures consistent with our results. Experimental deviations from theory were 0.1–0.3‰ in Δ_{36}, similar to our stated measurement uncertainty; therefore, at most, high-temperature isotope exchange occurred at 10% the rate of gas-phase oxygen-isotope exchange. Isotope effects in other reactions involving excited-state species (e.g., $O(^1D)$ and $O_2(^1\Delta_g)$) could also lead to deviations from isotopic equilibrium, but this system appears to be dominated by of $O(^3P) + O_2$ isotope exchange reactions. Future experiments with UV photolysis of O_2 and O_3 may yield further insight.

5. $^{18}O^{18}O$ and $^{17}O^{18}O$ in Tropospheric Air

5.1. Measurements

[41] We measured Δ_{36} and Δ_{35} in ~20 cm^3 samples of tropospheric air collected at the UCLA Court of Sciences in October 2011. Our measurements yield Δ_{36} = 2.05 ± 0.24‰ and Δ_{35} = 1.4 ± 0.5‰ (2σ; see Table 4), where quoted uncertainties reflect propagation of both random and systematic errors in the analysis. Reproducibility between sample preparations is ±0.08‰ and ±0.2‰ for Δ_{36} and Δ_{35} (2 s.e., n = 5), respectively. This external precision includes

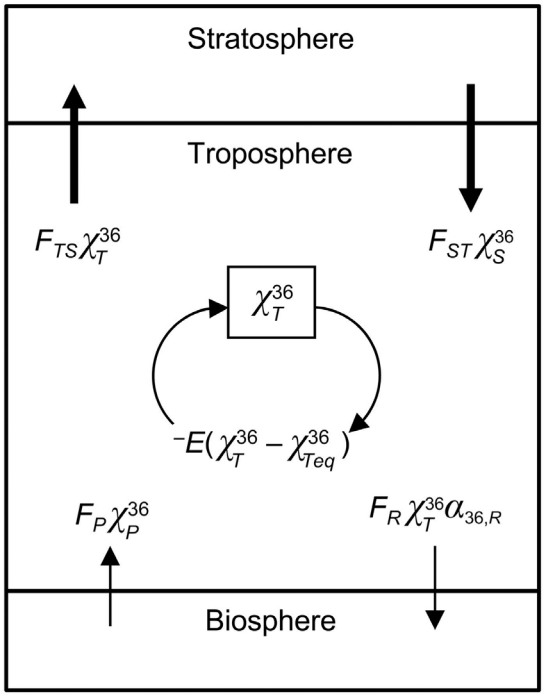

Figure 8. Schematic of box model showing the fluxes affecting χ_T^{36} from the stratosphere and the biosphere.

the corrections for residual ^{36}Ar and relatively small composition-dependent nonlinearity (see Appendix B).

[42] Atmospheric O_2 is in a non-equilibrium steady state between oxygen photosynthesis and respiration. Its bulk oxygen-isotope composition ($\delta^{18}O$ = 23–24‰) reflects biosphere processes on millennial timescales [*Bender et al.*, 1994], plus a small contribution (~0.3‰ in $\delta^{18}O$) from stratospheric photochemistry and subsequent oxygen-isotope transfer to CO_2 [*Yung et al.*, 1991; *Luz et al.*, 1999; *Luz and Barkan*, 2011]. Most of the $\delta^{18}O$ enrichment in atmospheric O_2 arises from respiration, but its effects on Δ_{36} and Δ_{35} are not known because $\beta_{36/34}$ and $\beta_{35/34}$ values for respiration have not yet been measured.

[43] The effects of photosynthesis and respiration on Δ_{36} and Δ_{35} could be rendered insignificant, however, even when the biosphere dominates the bulk isotopic budget, if isotopic reordering of the atmospheric O_2 reservoir occurs on timescales shorter than O_2 cycling through the biosphere. Therefore, one must consider the role of $O(^3P) + O_2$ isotope exchange reactions in the bond-ordering budget of atmospheric O_2. As we showed in Sections 2 and 4.2, $O(^3P) + O_2$ isotope exchange reactions can drive Δ_{36} and Δ_{35} toward equilibrium values in a closed system with a negligible effect on the bulk isotopic composition of O_2 in that system. The atmosphere, too, can be considered a closed system with respect to the oxygen isotopes in O_2 on sub-millenial timescales, with a O_2/O_3 mass balance yielding $\delta^{18}O$, $\Delta^{17}O \leq$ 0.3‰ [*Luz et al.*, 1999; *Young et al.*, 2002; *Luz and Barkan*, 2011]. Our reported tropospheric Δ_{36} and Δ_{35} values are consistent with isotopic equilibrium near 255 K, which is similar to the globally averaged tropospheric temperature of 251 K [*Vinnikov and Grody*, 2003], but $O(^3P) + O_2$ isotope exchange in the stratosphere probably has an influence on the tropospheric budget. Ultimately, a full consideration of the atmospheric Δ_{36} and Δ_{35} budgets will require an accounting of the biosphere's effects as well. We will evaluate not only the relative rates of isotope-exchange and biological processes, but also the range of expected biological fractionations, in Section 5.2, with the aim of presenting testable hypotheses for future study.

5.2. Model for $^{18}O^{18}O$ and $^{17}O^{18}O$ in the Atmosphere

[44] We constructed a model of the atmosphere to investigate the balance of photosynthesis, respiration, and $O(^3P) + O_2$ isotope exchange on the bond-ordering budget for O_2 in the troposphere. The mole fraction of $^{18}O^{18}O$ in the troposphere, χ_T^{36}, at steady state, can be described by the mass balance equation:

$$F_{ST}\chi_S^{36} - F_{TS}\chi_T^{36} + F_P\chi_P^{36} - F_R\chi_T^{36}\alpha_{36,R} - E\left(\chi_T^{36} - \chi_{T,eq}^{36}\right) = 0 \quad (14)$$

In equation (14), χ_P^{36} is the oxygen fraction of $^{18}O^{18}O$ for the photosynthetic end-member, $\alpha_{36,R}$ is the respiratory fractionation factor, and χ_{Teq}^{36} and χ_S^{36} are the oxygen fractions of $^{18}O^{18}O$ for the tropospheric-equilibrium and stratospheric mixing end-members, respectively. The downward (F_{ST}) and upward (F_{TS}) stratosphere-troposphere fluxes are in balance, i.e., $F_{ST} = F_{TS} = 4.9 \times 10^{18}$ mol O_2 yr^{-1} [*Appenzeller et al.*, 1996; *Hoag et al.*, 2005], as are the photosynthetic (F_P) and respiratory (F_R) fluxes, i.e., $F_P = F_R = 3.0 \times 10^{16}$ mol O_2 yr^{-1} [*Luz et al.*, 1999; *Blunier et al.*, 2002]. We have also included E, the rate of O_2 equilibration in the troposphere (in mol O_2 yr^{-1}), in the mass balance equation. Inclusion of this term is supported by predictions of an $O(^3P)$ concentration of order 10^3 cm^{-3}, constrained by tropospheric NO_x and O_3 concentrations [*Brasseur et al.*, 1990; *Liang et al.*, 2006]. A summary of model parameters can be found in Figure 8 and Table 5. Similar mass balance equations can be written for all the other O_2 isotopologues and are not shown here.

[45] In the following sections, we will discuss the likely consequences of the transport of stratospheric air (5.2.1), tropospheric isotope exchange reactions (5.2.2), and biological processes (5.2.3) on the tropospheric budget of Δ_{36}. We then conduct a sensitivity test (5.2.4) to determine the primary influences on tropospheric Δ_{36}. The arguments that follow will also be valid for Δ_{35}, but we will confine our discussion to Δ_{36} because of better analytical precision in our measurements. For simplicity, we have omitted the loss of ^{18}O and ^{17}O atoms from the O_2 reservoir via $O(^1D) + CO_2$ isotope exchange in the stratosphere, which should decrease $\delta^{18}O$ and $\delta^{17}O$ by ~0.3‰ [*Luz et al.*, 1999; *Luz and Barkan*, 2011]; while the primary source of stratospheric $O(^1D)$, O_3 photolysis, affects the O_2 mass balance, the $O(^1D) + CO_2$ reaction does not generate additional bond-ordering fractionation because it does not involve O_2.

5.2.1. Flux of High-Δ_{36} O_2 From the Stratosphere

[46] First, we estimate the stratospheric end-member, χ_S^{36}, which is expected to be an equilibrium-like value facilitated by $O(^3P) + O_2$ isotope exchange reactions. High $O(^3P)$ and O_2 concentrations in the stratosphere suggest that $O(^3P) + O_2$ isotope exchange occurs there readily (see Figure 9): Average expected chemical lifetimes of O_2 with respect to

Table 5. Description of Model Parameters

Parameter	Description	Value	Source
F_{ST}	Flux from stratosphere to troposphere	4.9×10^{18} mol O_2 yr^{-1}	*Appenzeller et al.* [1996], *Hoag et al.* [2005]
F_{TS}	Flux from troposphere to stratosphere	4.9×10^{18} mol O_2 yr^{-1}	*Appenzeller et al.* [1996], *Hoag et al.* [2005]
F_P	Flux out of biosphere from photosynthesis	3.0×10^{16} mol O_2 yr^{-1}	*Luz et al.* [1999], *Blunier et al.* [2002]
F_R	Flux into biosphere due to respiration	3.0×10^{16} mol O_2 yr^{-1}	*Luz et al.* [1999], *Blunier et al.* [2002]
E	Tropospheric Δ_n equilibration rate	$k_{O+O2}[O_2]_{avg}[O(^3P)]_{avg} \times V_{troposphere}$	This study
χ_S^{36}	Fraction of $^{18}O^{18}O$ in stratospheric O_2	See section 4.4.1 (Δ_{36} = 3.0‰)	This study
χ_T^{36}	Fraction of $^{18}O^{18}O$ in tropospheric O_2	See section 4.3 (Δ_{36} = 2.05‰)	This study
χ_{Teq}^{36}	Fraction of $^{18}O^{18}O$ in O_2 at isotope-exchange equilibrium in the troposphere	See section 4.4.2 (Δ_{36} = 1.7–2.1‰)	This study
$\alpha_{36,R}$	$^{18}O^{18}O/^{16}O^{16}O$ fractionation for respiration	See section 4.4.3	This study

oxygen isotope exchange, τ_{O2}, range from 160 days at 15 km to several minutes at 50 km (see Figure 2) [*Brasseur et al.*, 1990; *Wiegell et al.*, 1997; *Brasseur and Solomon*, 2005]. These short τ_{O2} times suggest that a typical air parcel, which upwells into the $O(^3P)$-rich stratosphere at tropical latitudes, will have its O-O bonds re-ordered before it re-enters the $O(^3P)$-poor troposphere in the middle and high latitudes >1 year later [*Holton et al.*, 1995; *Plumb*, 2007; *Engel et al.*, 2009; *Holzer et al.*, 2012]. O_2 chemistry involving other short-lived species (e.g., HO_x, NO_x, and ClO_x) may have a minor influence. Because rates of transport across the tropopause are generally much slower than rates of $O(^3P) + O_2$ isotope exchange, we expect that Δ_{36} and Δ_{35} will be temperature-stratified until a "horizon" is reached where the timescale of stratosphere-troposphere exchange (STE) is much shorter than that of isotopic equilibration at the in situ temperature. This isotope-exchange horizon probably lies in the climatological tropopause layer (~15 km; T = 190–200 K), where τ_{O2} is comparable to the dynamical STE lifetime of days to months. A descent velocity of 0.2–0.4 mm s^{-1} from stratospheric residual circulation at the midlatitude tropopause [*Rosenlof*, 1995] implies that the average sinking air parcel descends 1 km altitude in 30–60 days ($\Delta T \sim$ 5 K, or 0.1‰ in Δ_{36}). This transit time, τ_{1km}, is comparable to τ_{O2} between 15–20 km ($T \sim$ 200 K).

[47] We therefore estimate that O_2 entering the troposphere from the stratosphere has χ_S^{36} and χ_S^{35} corresponding to $\Delta_{36,S}$ = 3.0‰ and $\Delta_{35,S}$ = 1.6‰, the equilibrium values at $T \sim$ 200 K. While our predicted value is uncertain due to a simplified STE scheme ignoring seasonal variations and isentropic STE [*Holton et al.*, 1995], isotope-exchange lifetimes of less than a day above 25 km suggest that air entering the troposphere from the stratosphere is unlikely to have Δ_{36} values lower than 2.7‰. Furthermore, the effects of a changing ^{18}O and ^{17}O inventory in the O_2/O_3 system are limited because sequestration of oxygen isotopes in CO_2 via $O(^1D) + CO_2$ isotope-exchange reactions occurs much more slowly in the stratosphere than $O(^3P) + O_2$ isotope exchange (due to low $O(^1D)$ and CO_2 concentrations [*Yung et al.*, 1991; *Boering et al.*, 2004; *Liang et al.*, 2007]). Future measurements of stratospheric air, combined with 2-D modeling of intrastratospheric transport, should provide a more accurate stratospheric end-member. Note that the STE flux of 4.9×10^{18} mol O_2 yr^{-1} [*Appenzeller et al.*, 1996; *Hoag et al.*, 2005] would cycle through a mass of O_2 equivalent to the atmospheric inventory (3.7×10^{19} mol O_2) in 7.6 years; autocatalytic oxygen-isotope exchange in the stratosphere would therefore alter the tropospheric O_2 bond-ordering signature on decadal timescales.

5.2.2. Gas-Phase Isotope-Exchange Reactions in the Troposphere

[48] In the troposphere, $O(^3P)$ chemistry could drive Δ_{36} and Δ_{35} toward equilibrium values at tropospheric temperatures. The troposphere's equilibrium $^{18}O^{18}O$ and $^{17}O^{18}O$ fractions in O_2, χ_{Teq}^{36} and χ_{Teq}^{35}, might reflect the global

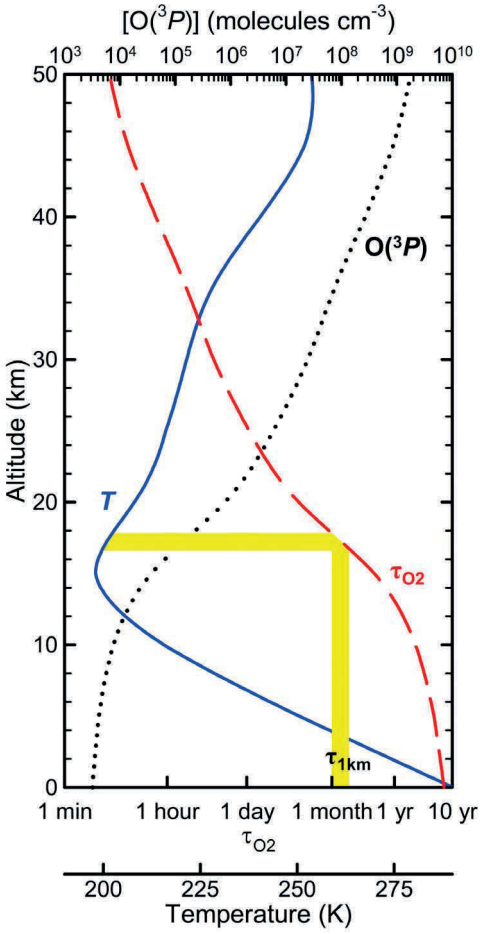

Figure 9. Temperature, $O(^3P)$, and τ_{O2} profiles derived from *Brasseur and Solomon* [2005]. $O(^3P)$ and τ_{O2} below 15 km are considered highly uncertain. Also shown (yellow area) is the estimated τ_{1km} range for downwelling stratospheric air (30–60 days), which implies a stratospheric $O(^3P) + O_2$ exchange horizon at 15–20 km.

average tropospheric temperature of 251 K (Δ_{36} = 2.1‰ and Δ_{35} = 1.1‰ [*Vinnikov and Grody*, 2003]) because the troposphere is well-mixed on timescales of about a year. The main tropospheric $O(^3P)$ source, NO_2, however, is emitted primarily at the surface by combustion processes and biological denitrification. NO_2 is also produced by lightning above the planetary boundary layer (1–3 km). At the surface, the photochemical NO_2 lifetime is several hours, significantly less than the timescale of mixing across the planetary boundary layer (~1 week). The presence of that vertical transport barrier suggests that Δ_{36} and Δ_{35} may be sensitive to the vertical distribution of NO_2. Weighting the tropospheric temperature profile by a vertical profile of NO_2 would yield an effective temperature of 281 K (Δ_{36} = 1.7‰ and Δ_{35} = 0.9‰). In any case, tropospheric $O(^3P)$ concentrations are related to E using known isotope-exchange rate coefficients ($k_{O+O2} \sim 3 \times 10^{-12}$ cm^3 s^{-1} [*Wiegell et al.*, 1997]), O_2 concentrations, and an estimate of the volume of the troposphere ($V_{troposphere} \approx 7.7 \times 10^9$ km^3):

$$E \approx k_{O+O2}[O_2]_{avg}\left[O\left(^3P\right)\right]_{avg} \times V_{troposphere} \quad (15)$$

Using this equation, $[O(^3P)]_{avg} = 1 \times 10^3$ cm^{-3}, $[O_2]_{avg} = 4.0 \times 10^{18}$ cm^{-3}, and 12 h of photochemistry each day, tropospheric $O(^3P)$ + O_2 isotope exchange cycles through 2.4×10^{18} mol O_2 per year, or a mass equivalent to the atmospheric O_2 inventory in 15 years.

5.2.3. O_2 Flux to and From the Biosphere

[49] The annual flux of O_2 to and from the biosphere, at ~1/160 the size of the STE flux [*Luz et al.*, 1999; *Hoag et al.*, 2005], may only be a minor contribution to the tropospheric Δ_{36} and Δ_{35} budgets. Still, the potential fractionations associated with the biosphere are important. Water oxidation during photosynthesis may yield O_2 with χ_P^{36} and χ_P^{35} near the stochastic distribution because photosynthesis does not discriminate between oxygen isotopes [*Guy et al.*, 1993; *Helman et al.*, 2005]. Moreover, O_2 cannot inherit a bond-ordering signature from water because H_2O contains no O-O bonds. Respiration leaves the O_2 residue between 10 and 30‰ enriched in $\delta^{18}O$ with a mass dependence $\beta_{34/33} \approx 0.516$ [*Lane and Dole*, 1956; *Guy et al.*, 1989; *Kiddon et al.*, 1993; *Angert et al.*, 2003; *Helman et al.*, 2005]. These fractionations resemble those of closed-system Knudsen diffusion ($\beta_{34/33}$ = 0.512), which would lead to $\chi_T^{36}\alpha_{36,R}$ and $\chi_T^{35}\alpha_{35,R}$ that are depleted relative to the stochastic distribution in the residue (i.e., $\Delta_{36} \approx -2$‰ and $\Delta_{35} \approx -1$‰ using $\beta_{36/34}$ = 0.52 and $\beta_{35/34}$ = 0.68; see Section 2.3). Oxygen consumption during photosynthesis, and possible associated oxygen-atom recycling in certain autotrophs [*Eisenstadt et al.*, 2010], could therefore alter the effective photosynthetic abundances, χ_P^{36} and χ_P^{35}, coming from aquatic environments. Nonetheless, the overall biosphere signature likely yields Δ_{36}, $\Delta_{35} < 0$. Laboratory experiments identifying the bond-ordering signatures of photosynthesis and respiration will allow one to constrain further their contributions to the atmospheric Δ_{36} and Δ_{35} budgets.

5.2.4. Interpretation of $^{18}O^{18}O$ Measurements

[50] We tested the sensitivity of the tropospheric Δ_{36} budget to various fractionations using our box model (equation (14) and Figure 8) and the fluxes and mixing end-members justified in the preceding sections. The simplified biosphere in the model, with photosynthetic O_2 having a bulk isotopic composition $\delta^{18}O$ = 4‰ and $\alpha_{34,R}$ = 0.98 (ε = −20‰), yielded a steady state $\delta^{18}O$ = 24.4‰. Subtracting 0.3‰ due to O-atom transfer to CO_2 in the stratosphere yields $\delta^{18}O$ = 24.1‰, similar to previous measured and modeled values [*Barkan and Luz*, 2005; *Luz and Barkan*, 2011]. While our measured $\delta^{18}O$ of O_2 is less than this value (see Table 1), the difference is attributable to the assumed bulk isotopic composition in our primary standard (San Carlos Olivine, $\delta^{18}O$ = 5.2‰). The interpretation of Δ_{36} is not affected by this subtle difference in bulk isotopic composition between model and the data.

[51] First, we will consider the biosphere alone in the absence of gas-phase bond-ordering equilibration due to $O(^3P)$ + O_2 isotope exchange reactions. Using χ_P^{36} corresponding to the stochastic distribution, the measured tropospheric Δ_{36} value (+2.05‰) can only be obtained with $\beta_{36/34}$ = 0.476 for respiration, which is a value lower than the theoretical limit for gas-phase kinetic processes involving O_2 [*Young et al.*, 2002] and much lower than the value suggested in Section 5.2.3. Moreover, after including the effects of $O(^3P)$ + O_2 isotope exchange in the stratosphere, respiration alone was unable to balance the flux of χ_S^{36} from the stratosphere for any value of $\beta_{36/34}$; the STE flux is too large. Increasing the biosphere-atmosphere flux of O_2 only yields modest decreases in tropospheric Δ_{36} (e.g., 2.7‰ for tenfold increases in F_R and F_P versus 3.0‰ for the base estimate). Alternately, χ_P^{36} would need to yield photosynthetic O_2 with $\Delta_{36} \sim -160$‰ (when $\beta_{36/34}$ = 0.515 for respiration) to balance the high-Δ_{36} air entering the troposphere from the stratosphere. Given that primary O_2 evolution does not discriminate between $^{16}O^{16}O$, $^{16}O^{17}O$, and $^{16}O^{18}O$ [*Guy et al.*, 1993; *Helman et al.*, 2005], a 160‰ disparity between $^{18}O^{18}O$ and $^{16}O^{18}O$ is implausible.

[52] Including tropospheric $O(^3P)$ + O_2 isotope exchange, however, can balance the STE flux of high-χ_S^{36} air. To explain $\Delta_{36} \leq 2.29$‰, the 2σ upper limit to our measured tropospheric Δ_{36}, E must be $\geq 2 \times 10^{19}$ mol O_2 yr^{-1}, corresponding to $[O(^3P)]_{avg} \geq 4 \times 10^3$ cm^{-3}. A vertical gradient in tropospheric $O(^3P)$ would alter these estimates: Weighting the tropospheric temperature profile by a vertical profile of NO_2 (see Section 5.2.2), yields $E = 0.6 - 5 \times 10^{19}$ mol O_2 yr^{-1}, and $[O(^3P)]_{avg} = 1 - 10 \times 10^3$ cm^{-3} can explain the entire 2σ range in measured Δ_{36}. A similar tropospheric $O(^3P)$ concentration range is obtained even if we use our lower estimate of χ_S^{36} corresponding to Δ_{36} = 2.7‰ coming from the stratosphere. These $O(^3P)$ concentrations, derived using our two-box model, are thus consistent with global models [*Brasseur et al.*, 1990; *Brasseur and Solomon*, 2005; *Liang et al.*, 2006].

[53] Based on our analysis of Δ_{36} and Δ_{35}, $O(^3P)$ + O_2 isotope exchange appears to exert the primary influence on isotopic bond ordering in tropospheric O_2. While the effects of O_2 production and consumption by the biosphere are yet to be determined, gas-phase chemistry in the stratosphere and troposphere is sufficient to explain our measured value of Δ_{36} in tropospheric air. Future detailed studies on Δ_{36} and Δ_{35} in stratospheric O_2, photochemistry, and isotopic

fractionations associated with the biosphere will lay the groundwork for applications relevant to the atmospheric chemistry and biogeochemical cycling of O_2.

6. Conclusions and Outlook

[54] We have measured proportional enrichments in $^{18}O^{18}O$ and $^{17}O^{18}O$ of 2.05 ± 0.24‰ and 1.4 ± 0.5‰ (2σ), respectively, in tropospheric air. Based on our laboratory experiments and a box model for atmospheric O_2, we hypothesize that these enrichments are primarily driven by $O(^3P)$ + O_2 isotope-exchange reactions occurring in the stratosphere and troposphere. Due to the sensitivity of tropospheric Δ_{36} on the STE flux, atmospheric temperature profile, and $O(^3P)$ concentration, we hypothesize that measurements of bond ordering in tropospheric O_2 may be able to constrain atmospheric dynamics and free-radical chemistry in the present, and perhaps also in the past.

[55] Temporal variations in Δ_{36} and Δ_{35} in the ice core record, specifically, may trace anthropogenic and climate-driven changes in atmospheric chemistry and circulation on decadal timescales. For instance, the main sources of tropospheric $O(^3P)$ were greatly reduced, relative to today, during preindustrial times: NO_x emissions have been estimated to be as little as one-fifth those of the present-day, while tropospheric O_3 concentrations may also have been reduced by half [*Thompson*, 1992; *Martinerie et al.*, 1995]. Lower tropospheric $O(^3P)$ concentrations would decrease the tropospheric bond-ordering equilibration rate (E in equation (14) and Figure 8), shifting the steady state tropospheric Δ_{36} value up toward the stratospheric mixing end-member value. A fivefold reduction in tropospheric $O(^3P)$ could result in as much as a 0.5‰ increase in tropospheric Δ_{36} relative to the present-day value, depending on the effective tropospheric temperature used for χ^{36}_{Teq} and assuming no change in the STE flux. A recent prediction of only modest changes to tropopause temperature (~+1°C) and STE flux during the Last Glacial Maximum could potentially also be tested [*Rind et al.*, 2009].

[56] The triple-isotopologue mass dependences, $\beta_{36/34}$ and $\beta_{35/34}$, may also be used to constrain the oxygen budget in closed systems such as soils [*Aggarwal and Dillon*, 1998; *Lee et al.*, 2003] and the ocean's interior [*Kroopnick and Craig*, 1976; *Bender*, 1990]. Bulk isotopic fractionations of up to +15‰ have been observed, which would result in a change of −1.3‰ in Δ_{36} of the residue (using $\beta_{36/34}$ = 0.522). Over this range in bulk isotopic composition, a $\beta_{36/34}$ difference of 0.002 would result in a 0.1‰ difference in Δ_{36}. These triple-isotopologue β values provide additional information that augments the "triple-isotope" $\beta_{34/33}$ values (i.e., relating $\delta^{18}O$ and $\delta^{17}O$) used to partition oxygen consumption fluxes into their component mechanisms [*Angert and Luz*, 2001; *Young et al.*, 2002; *Angert et al.*, 2003], and may prove valuable where oxygen cycling mechanisms are poorly understood. Interpreting measured Δ_n values using mass-dependent fractionation laws represents a general approach to multi-isotopologue systematics that can be applied to any environment where single-phase isotope-exchange equilibration is not the dominant process. The sensitivity of Δ_{36} and Δ_{35} to diffusion, and not gravitational fractionation, for example, may comprise a test of physical fractionation mechanisms in glacial firn and ice layers, including countercurrent flux [*Severinghaus et al.*, 1996] and bubble close-off [*Severinghaus and Battle*, 2006].

[57] Finally, this study highlights the potential value of high-resolution gas-source IRMS instruments for understanding atmospheric systems. Our analyses of $^{18}O^{18}O$ and $^{17}O^{18}O$ in O_2 were possible on a low-resolution IRMS only after significant sample preparation and mass spectrometry of large gas samples. High-resolution instruments may be able to resolve $^{18}O^{18}O$ from ^{36}Ar well enough to reduce the sample handling artifacts and instrumental ion corrections that ultimately limit the precision in the present study. Detailed analyses of these species in O_2 trapped in ice cores, or in low-O_2 zones in the oceans, will likely require sensitivity and precision higher than what is currently available.

Appendix A: β-Values That Preserve Δ_{36} and Δ_{35}

[58] Here, we derive the triple-isotopologue mass dependences $\beta_{36/34}$ and $\beta_{35/34}$ that preserve Δ_{36} and Δ_{35} values. We will omit the contribution of $^{17}O^{17}O$ to mass-34 O_2 for simplicity, as the errors it imposes on Δ_{36} and Δ_{35} in the case of gravitational fractionation are $<10^{-6}$ ‰. References to mass-34 O_2 herein describe $^{16}O^{18}O$ species exclusively.

[59] During an arbitrary fractionation process, isotopologue abundances change from R_i to R_f according to α values for each isotopologue relative to $^{16}O^{16}O$:

$$^{36}R_f = {}^{36}R_i \times \alpha_{36} \tag{A1a}$$

$$^{35}R_f = {}^{35}R_i \times \alpha_{35} \tag{A1b}$$

$$^{34}R_f = {}^{34}R_i \times \alpha_{34} \tag{A1c}$$

$$^{33}R_f = {}^{33}R_i \times \alpha_{33}. \tag{A1d}$$

In most cases, O_2 is near natural abundance and the ^{18}O and $^{16}O^{18}O$ α values are comparable, yielding

$$^{18}R_f \cong {}^{18}R_i \times \alpha_{34} \tag{A2a}$$

$$^{17}R_f \cong {}^{17}R_i \times \alpha_{33} \tag{A2b}$$

The stochastic distributions for $^{18}O^{18}O$ and $^{17}O^{18}O$ in gases with composition R_f are therefore

$$^{36}R_{f,stochastic} = \left({}^{18}R_f\right)^2 \tag{A3a}$$

$$\cong \left({}^{18}R_i \times \alpha_{34}\right)^2 \tag{A3b}$$

$$\cong \left({}^{36}R_{i,stochastic}\right)(\alpha_{34})^2 \tag{A3c}$$

$$^{35}R_{f,stochastic} = 2\times {}^{18}R_f\,{}^{17}R_f \tag{A4a}$$

$$\cong 2 \times \left({}^{18}R_i \times \alpha_{34}\right)\left({}^{17}R_i \times \alpha_{33}\right) \tag{A4b}$$

$$\cong \left({}^{35}R_{i,stochastic}\right)\alpha_{34}\alpha_{33} \tag{A4c}$$

according to equations (1a) and (A2a). Simple fractionation factors, $(\alpha_{34})^2$ and $\alpha_{34}\alpha_{33}$, relate the stochastic distribution of $^{18}O^{18}O$ and $^{17}O^{18}O$ in the initial population ($R_{i,stochastic}$) to that in the fractionated population ($R_{f,stochastic}$). Dividing equation (A1a) by equation (A3c), and equation (A1b) by equation (A4c), yields:

$$\alpha_{34} = (\alpha_{36})^{1/2} \tag{A5}$$

$$\alpha_{34} = \frac{\alpha_{35}}{\alpha_{33}} \tag{A6}$$

for a gas with $R_f/R_{f,stochastic} = R_i/R_{i,stochastic}$ (i.e., Δ_{36} and Δ_{35} values unchanged upon fractionation from R_i to R_f). Equation (A5) then resembles equation (3) with $\beta_{36/34} = 0.500$; therefore, $\beta_{36/34} = 0.500$ preserves Δ_{36} as it is defined in equation (2b). Finally, we recognize that the $\beta_{35/34}$ preserving Δ_{35} depends on the "triple-isotope" mass dependence $\beta_{34/33}$: Values of $\beta_{35/34}$ between 0.667 and 0.654 preserve Δ_{35} for specific values of $\beta_{34/33}$ between 0.500 and 0.530, respectively, a range in $\beta_{34/33}$ spanning equilibrium, kinetic, and gravitational fractionation [*Young et al.*, 2002].

[60] For a gas in a gravitational potential (equation (5)), α values depend on the mass differences between isotopologues:

$$m_{34}–m_{32} = (m_{18} + m_{16})–(m_{16} + m_{16}) \tag{A7a}$$

$$= (m_{18}–m_{16}) \tag{A7b}$$

$$m_{36}–m_{32} = (m_{18} + m_{18})–(m_{16} + m_{16}) \tag{A8a}$$

$$= 2 \times (m_{34}–m_{32}) \tag{A8b}$$

Similarly,

$$m_{33}–m_{32} = (m_{17}–m_{16}) \tag{A9}$$

$$m_{35}–m_{32} = (m_{33}–m_{32}) + (m_{34}–m_{32}). \tag{A10}$$

Therefore,

$$\alpha_{36,gravitation} = e^{(m_{36}-m_{32})\frac{gZ}{R_G T}} \tag{A11a}$$

$$= e^{2(m_{34}-m_{32})\frac{gZ}{R_G T}} \tag{A11b}$$

$$= \left(\alpha_{34,gravitation}\right)^2, \tag{A11c}$$

and

$$\alpha_{35,gravitation} = e^{(m_{35}-m_{32})\frac{gZ}{R_G T}} \tag{A12a}$$

$$= e^{\left[(m_{34}-m_{32})+(m_{33}-m_{32})\right]\frac{gZ}{R_G T}} \tag{A12b}$$

$$= \alpha_{34,gravitation}\alpha_{33,gravitation}. \tag{A12c}$$

Equation (A11c) is identical to equation (A5), while equation (A12c) is identical to equation (A6). Therefore, gravitational fractionation preserves both Δ_{36} and Δ_{35}, with $\beta_{36/34} = 0.500$, $\beta_{34/33} = 0.501$, and $\beta_{35/34} = 0.666$.

Appendix B: Mass Spectrometry

B1. Instrument Protocols

[61] Purified O_2 samples were analyzed on a dual-inlet Thermo-Finnigan MAT 253 IRMS equipped with 9 Faraday cups. The gas was equilibrated with the IRMS's sample bellows at ~240°C for 35 min. Passive equilibration yielded analyses that consistently fractionated light (0.3–1‰ in $\delta^{18}O$) relative to their known bulk isotopic composition. Therefore, we "mixed" the gas by alternating the bellows volume between 25% and 100% three times every 200 s during the equilibration. An operating system script was written to automate this task, which eliminated the bulk isotopic fractionation (<0.02‰ in $\delta^{18}O$).

[62] Two of the Faraday cups had wide geometries to accommodate multicollection of O_2 and CO_2 on the same detector array. Amplifier resistor values of 5×10^7, 1×10^{11}, 1×10^{10}, 3×10^{11}, and 1×10^{12} Ω yielded nominal detection voltages of 4000, 5500, 3500, 45, and 400 mV at $m/z = 32$ (wide cup), 33, 34 (wide cup), 35, and 36, respectively, with an ion-source pressure of ~2.5×10^{-7} mBar. A 3×10^{11}-Ω resistor was used for $m/z = 35$ detection because we identified an electronic noise source coming from a switch on its amplifier board, particular to this Faraday cup-amplifier configuration, which degraded the signal-to-noise ratio (SNR) at higher resistor values; the 3×10^{11}-Ω resistor on the $m/z = 35$ amplifier board yielded a SNR similar to that of a 1×10^{12}-Ω resistor on a switchless board. The resulting lower voltage on $m/z = 35$ was therefore the most sensitive to inaccuracies arising from long-term electronic drifts of order 1 mV (e.g., electronic offsets).

[63] Our working standard gas had a bulk isotopic composition of $\delta^{18}O = -12.404$‰ and $\delta^{17}O = -6.457$‰ against Vienna Standard Mean Ocean water, calibrated by assuming that San Carlos Olivine has a composition $\delta^{18}O = 5.200$‰ and $\delta^{17}O = 2.742$‰.

[64] Sample peak shapes are shown in Figure B1. Under typical ion-source pressures, we observed that all the minor ion beams had negative, pressure-sensitive baselines, or "pressure baselines," that reduced the observed voltage relative to its true value. The magnitudes of these baselines varied with source pressure, conductance (modulated by the position of the "sulfur window"), extraction, and various tuning parameters, and they are qualitatively different from the zero-analyte backgrounds that were routinely subtracted as part of typical measurements. In general, these pressure baselines were negligible for $m/z = 33$ and 34 (−6 and −2 mV, respectively, resulting in errors of order 0.001‰ in $\delta^{17}O$ and $\delta^{18}O$), but significant for $m/z = 35$ and 36 (about −18 and −75 mV, respectively). They were affected by the presence of a strong magnetic field (i.e., a rare earth magnet) near the inlet to the Faraday cups. Secondary electrons inadequately quenched by the Faraday-cup electron suppressors and/or produced by collisions of ions with the sides of the IRMS flight tube are thought to be the source of these baselines.

[65] Pressure baselines were not of equal magnitude on either side of the molecular ion peaks. The high-voltage

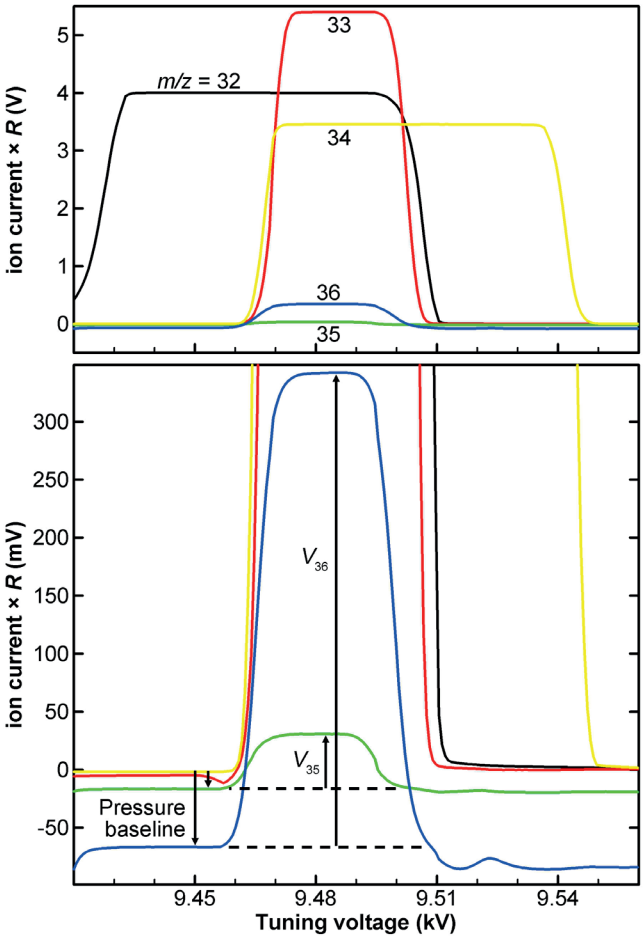

Figure B1. Two views of typical IRMS peak shapes for $m/z = 32$–36. Pressure baselines for $m/z = 35$ and 36 are shown in the zoomed view at bottom with arrows corresponding to the baseline-corrected V_{35} and V_{36} values.

(low-mass) side was typically more negative (see Figure B1). Placing a rare earth magnet on the flight tube near the detector array corrected this disparity, indicating that stray electron splatter may be its root cause. Measurements made with the magnet in place were consistent with those made without the magnet, albeit slightly noisier. Furthermore, the low-voltage (high-mass) side yielded the best reproducibility, so it was used, without the magnet, for pressure-baseline corrections.

[66] To measure these pressure baselines, we employed an acceleration-voltage-switching protocol similar to one being developed for measurements of mass-47 CO_2 [*He et al.*, 2012]. First, the sample and standard sides of the IRMS were pressure-balanced on $m/z = 32$ to within 15 mV at an acceleration voltage corresponding to the pressure baselines, i.e., 9.450 kV. Next, sample and standard pressure-baseline voltages for $m/z = 33$–36 were measured in three IRMS sample-standard measurement cycles. The acceleration voltage was then increased to a value corresponding to peaks in the analyte signal, i.e., 9.485 kV, for 10 IRMS measurement cycles. Last, the acceleration voltage was switched back to the previous pressure-baseline setting, and another three measurement cycles were taken. During each measurement cycle, sample and standard signals were each integrated for 10s after an idle time of 20s. Each acquisition block was composed of 6 pressure-baseline and 10 on-peak measurement cycles, yielding a total analysis time of ~25 min. Reported values are external averages and standard errors from 4–6 acquisition blocks.

[67] An example of the $m/z = 36$ signal during an acquisition block is shown in Figure B2. The pressure-baseline voltage increases (gets less negative), while the on-peak voltage decreases (gets less positive) with time; calculating the magnitude of the molecular signal requires that one account for both trends simultaneously. The pressure baseline was interpolated from a linear regression of the background voltage from the measurement cycles before and after the 10 on-peak measurement cycles. Separate linear regressions were generated for the sample and standard sides to mitigate errors due to sample-standard pressure imbalance. The molecular signal on each side for a measurement cycle was then calculated as the difference between the on-peak voltages and the interpolated pressure-baseline voltages. Signals at $m/z = 35$ were derived in the same way using its observed and pressure-baseline voltages.

[68] Signal hysteresis during the acceleration-voltage switching protocol is a potential concern; stray electronic capacitances of the order pF can increase the RC signal relaxation time, τ_{RC}, significantly from its nominal 2-s value on the $m/z = 36$ cup ($R = 1 \times 10^{12}$ Ω and $C = 2$ pF). If the electronic relaxation time exceeded the time in between switching, the contrast between the observed and pressure-baseline measurements would have been smaller than the true values, leading to a scale compression in the resulting Δ_{36} and Δ_{35} values. Using $\tau_{RC} = 2$ s and a 20-s idle time, we calculate that the signal contrast (i.e., $V_{36} \times \exp(20s/-\tau_{RC})$) will decrease by 0.045‰ at most in Δ_{36}, which is less than our reported precision. To evaluate if hysteresis was significant for our measurements, we tested a different method for calculating V_{36} that was sensitive to longer-term (minutes to hours) instrumental drifts rather than the shorter-term (seconds to minutes) drifts of concern for the procedure depicted in Figure B2. The alternate method used pressure-baseline trends that were measured as separate 10-cycle

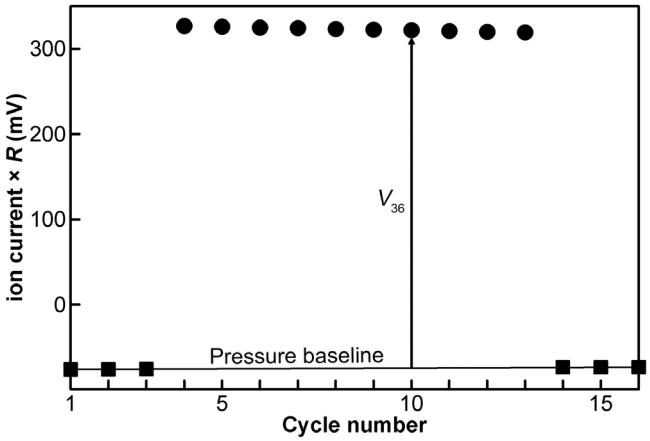

Figure B2. Signal at $m/z = 36$ during a 16-cycle acquisition block showing interpolated pressure baseline used to derive V_{36}.

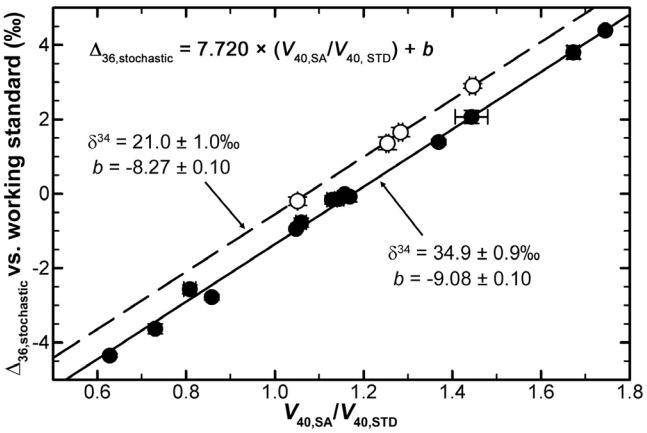

Figure B3. Argon-$\Delta_{36,stochastic}$ correction lines for O_2 of bulk composition δ^{34} = 34.9 ± 0.9‰ and 21.0 ± 1.0‰ (1σ), which are parallel within their linear-regression fit uncertainties.

acquisition blocks before and after every 2–3 blocks of on-peak measurements; the average linear regression values used to calculate V_{36} values. Results from both methods were consistent with one another within 0.1‰ in Δ_{36}.

B2. Ion Corrections for ^{36}Ar and Instrumental Nonlinearities

[69] A final ion correction for ^{36}Ar was applied during analyses of O_2 because it was still present at ppb levels in both the reference gas and in gas samples. This ion correction, dependent on both bulk isotopic composition (δ^{34}) and the m/z = 40 voltage ratio (sample/standard; $V_{40,SA}/V_{40,STD}$), was calculated by measuring the dependence of Δ_{36} versus $V_{40,SA}/V_{40,STD}$ for high-temperature gases of two different δ^{34} values (see Figure B3). To generate these ion-correction lines, standard gases were passed through the GC system with varied collection times. Longer collection times led to higher $V_{40,SA}/V_{40,STD}$ because more argon from the helium stream was collected (see Section 3.1) These lines constituted the high-temperature ($\Delta_{36} \sim \Delta_{35} \sim 0$) reference against which experimental samples were compared. Argon-corrected Δ_{36} values were obtained by taking the difference between the uncorrected Δ_{36} value and a high-temperature reference line at a given $V_{40,SA}/V_{40,STD}$.

[70] The argon correction lines for δ^{34} = 34.9 ± 0.9‰ and 21.0 ± 1.0‰ were offset, but parallel within the fit uncertainties of their respective linear regressions. Plotting the ordinate as an ion current instead of a Δ_{36} value yields similar results (not shown). These observations indicate the presence of a subtle nonlinearity between measured and actual Δ_{36} values over that range in δ^{34} that may be a general feature of 'clumped-isotope' analyses at high source pressures [*Huntington et al.*, 2009]. The small molecular signals in our analyses in particular, i.e., V_{36} < 500 mV may also be subject to amplifier nonlinearities. To account for these nonlinearities, we assumed that the slopes of the argon-correction lines (i.e., of Δ_{36} versus $V_{40,SA}/V_{40,STD}$) were invariant, and that their intercepts varied linearly with δ^{34}. We used the best fit δ^{34} = 34.9‰ slope (1 s.e., n = 13, r^2 = 0.9989, MSWD = 1.8) in the expression,

$$\Delta_{36,stochastic} = (7.720 \pm 0.075) \times \left(V_{40,SA}/V_{40,STD}\right) + b \quad \text{(B1)}$$

to find the intercepts, b, for the δ^{34} = 34.9‰ and 21.0‰ data (n = 4; r^2 = 0.9991, MSWD = 0.02; see Figure B3). The resulting relationship between b and δ^{34}, based on these two tie points, was

$$b = (-0.060 \pm 0.010) \times \delta^{34} - (7.02 \pm 0.35) \quad \text{(B2)}$$

after accounting for nonzero Δ_{36} of the two high-temperature standards, i.e., Δ_{36} = 0.03‰ and 0.02‰ at 800°C and 1000°C, respectively. Reported uncertainties are 1σ estimated using a Monte Carlo simulation (see section B3). The dependence of b on bulk isotopic composition is of an opposite sign from that which has been reported for Δ_{47} measurements [*Huntington et al.*, 2009; *Dennis et al.*, 2011], but it is of the same sign as that reported in another study in which pressure baselines were measured [*He et al.*, 2012].

[71] For an O_2 sample of a given δ^{34}, our reported Δ_{36} value was calculated using the equation:

$$\Delta_{36} = \Delta_{36 vs.working\ std} - \Delta_{36,stochastic} \quad \text{(B3)}$$

This equation can be used only when both terms in the difference correspond to the same bulk composition δ^{34}. Therefore, b was first calculated for the sample's δ^{34} (i.e., that for $\Delta_{36 vs.working\ std}$) using equation (B2), after which $\Delta_{36,stochastic}$ was calculated for the sample's $V_{40,SA}/V_{40,STD}$. Atmospheric O_2 had δ^{34} = 36.275 ± 0.080‰ (2 s.e.), close to one of our standard gases (δ^{34} = 34.9‰), where the nonlinearity correction was comparable to the 1σ total uncertainty in Δ_{36} (0.1‰).

[72] For our Knudsen diffusion experiment (Section 4.1), some uncertainty in Δ_{36} arises from the composition-dependent nonlinearity relationship derived in the previous section, because the bulk isotopic composition of both the diffused and residue populations were significantly (>10‰ in δ^{34}) outside the range for which high-temperature gases were available. Because of the relative difficulty in generating low-argon O_2 standards over a wider range of bulk isotopic composition, we are unable to include a larger range of bulk isotopic composition at this time. Still, we see excellent agreement, within our reported uncertainty, between our data and the model of the experiment using equation (12).

B3. Uncertainty Estimates

[73] To estimate the uncertainty in final Δ_{36} values associated with these ion-correction and nonlinearity relationships, which dominated the total uncertainty, we built a Monte Carlo simulation of equation (9). We sampled 100,000 points on each of 4 different Gaussian distributions corresponding to the δ^{34} (abscissa) and b (ordinate) values. Uncertainties in the slope and intercept of equation (B1) were calculated this way, as were $\Delta_{36,stochastic}$ uncertainties at specific $V_{40,SA}/V_{40,STD}$ values. These uncertainties were added in quadrature with the analytical standard error in $\Delta_{36 vs.working\ std}$ to obtain 1σ uncertainty limits for the final Δ_{36} values.

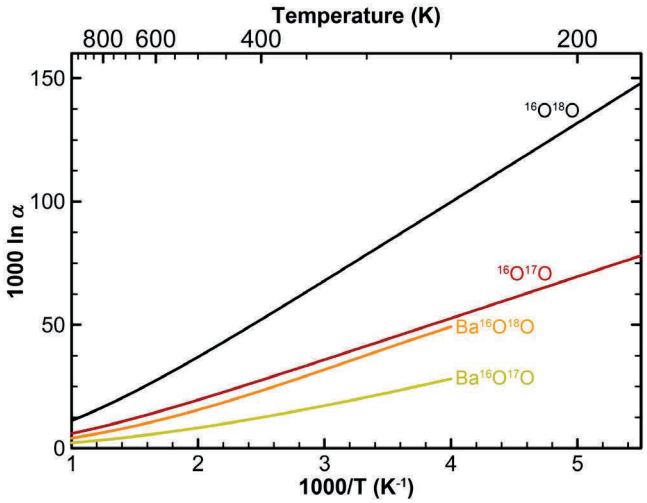

Figure C1. Calculated bulk isotopic fractionation for the BaO_2 and O_2 systems relative to atomic O vapor.

[74] For Δ_{35} measurements, an argon correction was not necessary because $m/z = 35$ is not isobaric with an argon isotope. In addition, a composition-dependent nonlinearity was not identified, perhaps because the analytical precision of individual measurements was ±0.2‰ (1σ s.e.); that uncertainty may exceed the magnitude of composition-dependent nonlinearity over our range in $\delta^{35} \sim$ 30–57‰. External (multisample) averages for high-temperature gases with $\delta^{35} = 51 \pm 1$‰ and 32 ± 2‰ (1 s.d.) yielded Δ_{35} values that were not significantly different from each other. Therefore, because we could not rule out a composition-dependent nonlinearity for Δ_{35}, we used 2 external standard errors as the uncertainty bounds for the high-temperature standard when propagating uncertainty in Δ_{35}. Higher-precision measurements of Δ_{35} should be possible with higher amplification on the $m/z = 35$ Faraday cup with a new detector array that does not have the SNR problems we experienced (see section B1).

Appendix C: BaO_2 Theory

[75] Equilibrium isotopic ordering in barium peroxide is estimated thermodynamically using the method of *Schauble et al.* [2006]. In this method, vibrational frequencies and zero-point energies are determined by Density Functional Theory (DFT), using the gradient-corrected PBE functional [*Perdew et al.*, 1996]. In order to simplify the DFT calculation, the electronic structure of each atom is approximated with a pseudopotential. An ultrasoft pseudopotential [*Vanderbilt*, 1990] is used for oxygen (pbe-rrjkus.UPF from http://www.quantum-espresso.org). A norm-conserving Rappe–Rabe–Kaxiras–Joannopoulos (RRKJ) type pseudopotential [*Rappe et al.*, 1990] was generated for barium using the OPIUM pseudopotential generator (http://opium.sourceforge.net/) and parameters from the Rappe group pseudopotential archive (maintained by Joe Bennett, http://www.sas.upenn.edu/rappegroup/htdocs/Research/PSP/ba.optgga1.param). The barium pseudopotential includes 5s, 5p, 5d and 6s shells in valence.

[76] All DFT calculations were made with the Quantum Espresso code [*Giannozzi et al.*, 2009] using a 50 Rydberg energy cutoff for the plane wave basis set. Electronic wave vectors in the Brillouin zone were sampled on a shifted 4 × 4 × 4 Monkhorst-Pack grid, and the phonon density of states was sampled using a shifted Monkhorst–Pack-like grid [*Gonze et al.*, 2002] with three distinct wave vectors. Calculated vibrational frequencies were scaled downward by 3.5% so that the peroxide O-O stretching mode frequency matched Raman measurements in BaO_2 (843 cm^{-1} [*Efthimiopoulos et al.*, 2010]). This scale factor ignores anharmonicity in both the model and the Raman measurement, which is expected to have small effects on isotopic ordering [*Wang et al.*, 2004; *Schauble et al.*, 2006; *Cao and Liu*, 2012]. Anharmonicity-corrected frequencies don't appear to be known for BaO_2.

[77] Trial calculations with higher plane wave cutoff energies and denser electronic wave vector grids yielded very similar energies and optimized crystal structures. The room temperature ^{18}O-^{18}O bond-ordering equilibrium calculated with a 1-wave vector phonon sample and different barium pseudopotential (Ba.pbe-nsp-van.UPF from http://www.quantum-espresso.org) are within ~0.01‰ of the present result, suggesting that the choice of barium pseudopotential is not critical. This is also consistent with the very low frequencies observed for all modes other than the O-O stretch; low-frequency modes are not expected to strongly affect isotopic ordering. The optimized crystal structure and frequencies of Raman-active vibrational modes are very close to those determined by a recent DFT study using projector-augmented waves [*Efthimiopoulos et al.*, 2010] Assuming anharmonicity of no more than a few percent in the O-O stretching mode, and that lattice modes do not contribute significantly to isotopic ordering in BaO_2, the calculated $^{18}O_2$ equilibrium might reasonably be expected to be accurate to ~0.02‰ to 0.03‰ at room temperature and above. Uncertainty in these calculations ought to scale with isotopologue mass, and therefore be correspondingly smaller for $^{17}O^{18}O$ and $^{17}O^{17}O$: ~0.01–0.02‰ and ~0.01‰, respectively.

[78] Below (see also Figure C1) are the polynomials fit to estimated isotopologue and isotopic equilibria using temperatures in Kelvin. BaO_2 equilibria were fit for T ≥ 250 K, and show a maximum misfit of 0.003‰. For clumped O_2 isotopic equilibria, the fits are for T ≥ 170 K with a maximum misfit of 0.004‰ in Δ_n values and 0.09‰ in α. BaO_2 (this study)

$$Ba^{16}O^{18}O + Ba^{16}O^{18}O \leftrightarrows Ba^{18}O^{18}O + Ba^{16}O^{16}O$$

$$K_{eq} \times 4 = \left(-7.5990 \times 10^{10}\right)T^{-6} + \left(2.7366 \times 10^{6}\right)T^{-4} + (2.9633)T^{-2} + 1 \quad \text{(C1a)}$$

$$Ba^{16}O^{17}O + Ba^{16}O^{18}O \leftrightarrows Ba^{17}O^{18}O + Ba^{16}O^{16}O$$

$$K_{eq} \times 2 = \left(-4.0330 \times 10^{10}\right)T^{-6} + \left(1.4422 \times 10^{6}\right)T^{-4} + (1.5856)T^{-2} + 1 \quad \text{(C1b)}$$

$$Ba^{16}O^{17}O + Ba^{16}O^{17}O \leftrightarrows Ba^{17}O^{17}O + Ba^{16}O^{16}O$$

$$K_{eq} \times 4 = \left(-2.1324 \times 10^{10}\right)T^{-6} + \left(7.5848 \times 10^{5}\right)T^{-4} + (0.85513)T^{-2} + 1 \quad \text{(C2a)}$$

$$\alpha_{18\text{-}16} = \left(1.0365 \times 10^{12}\right)T^{-6} - \left(6.3615 \times 10^{7}\right)T^{-4} + \left(4.1690 \times 10^{3}\right)T^{-2} + 1 \quad \text{(C2b)}$$

$$\alpha_{17\text{-}16} = \left(5.9074 \times 10^{11}\right)T^{-6} - \left(3.6056 \times 10^{7}\right)T^{-4} + \left(2.2105 \times 10^{3}\right)T^{-2} + 1 \quad \text{(C2c)}$$

O_2 (This study, adapted from *Wang et al.* [2004])

$$^{16}O^{18}O + {}^{16}O^{18}O \leftrightarrows {}^{18}O^{18}O + {}^{16}O^{16}O$$

$$K_{eq} \times 4 = \left(-4.30256 \times 10^{11}\right)T^{-6} + \left(9.07569 \times 10^{9}\right)T^{-5} - \left(7.21969 \times 10^{7}\right)T^{-4} + \left(2.47642 \times 10^{5}\right)T^{-3} - \left(1.85176 \times 10^{2}\right)T^{-2} + \left(4.56043 \times 10^{-2}\right)T^{-1} + 1 \quad \text{(C3)}$$

$$^{16}O^{17}O + {}^{16}O^{18}O \leftrightarrows {}^{17}O^{18}O + {}^{16}O^{16}O$$

$$K_{eq} \times 2 = \left(-2.28850 \times 10^{11}\right)T^{-6} + \left(4.80743 \times 10^{9}\right)T^{-5} - \left(3.80618 \times 10^{7}\right)T^{-4} + \left(1.29814 \times 10^{5}\right)T^{-3} - \left(9.61087 \times 10^{1}\right)T^{-2} + \left(2.34001 \times 10^{-2}\right)T^{-1} + 1 \quad \text{(C4)}$$

$$^{16}O^{17}O + {}^{16}O^{17}O \leftrightarrows {}^{17}O^{17}O + {}^{16}O^{16}O$$

$$K_{eq} \times 4 = \left(-1.21482 \times 10^{11}\right)T^{-6} + \left(2.54270 \times 10^{9}\right)T^{-5} - \left(2.00456 \times 10^{7}\right)T^{-4} + \left(6.80125 \times 10^{4}\right)T^{-3} - \left(4.98714 \times 10^{1}\right)^{-2} + \left(1.20347 \times 10^{-2}\right)T^{-1} + 1 \quad \text{(C5a)}$$

$$\alpha_{18\text{-}16} = \left(-1.3073 \times 10^{12}\right)T^{-6} + \left(4.7312 \times 10^{9}\right)T^{-5} + \left(2.4903 \times 10^{8}\right)T^{-4} - \left(3.0146 \times 10^{6}\right)T^{-3} + \left(1.4894 \times 10^{4}\right)T^{-2} - \left(9.1783 \times 10^{-1}\right)T^{-1} + 1 \quad \text{(C5b)}$$

$$\alpha_{17\text{-}16} = \left(-6.0449 \times 10^{11}\right)T^{-6} + \left(3.8369 \times 10^{8}\right)T^{-5} + \left(1.5213 \times 10^{8}\right)T^{-4} - \left(1.6937 \times 10^{6}\right)T^{-3} + \left(7.9791 \times 10^{3}\right)T^{-2} - \left(5.0833 \times 10^{-1}\right)T^{-1} + 1 \quad \text{(C5c)}$$

[79] **Acknowledgments.** We thank K. Ziegler and V. Brillo for experimental assistance, H. P. Affek, Q. Li, and C. Deutsch for helpful discussions, Y. L. Yung for providing a sample output from his atmospheric model, and the reviewers (J. Severinghaus and two anonymous others) for their comments on the manuscript. This research was supported by the National Science Foundation Earth Sciences Postdoctoral program (EAR-1049655 to L.Y.Y.), grant EAR-0961221 to E.D.Y., and grant EAR-1047668 to E.A.S.

References

Affek, H. P., and J. M. Eiler (2006), Abundance of mass-47 CO_2 in urban air, car exhaust and human breath, *Geochim. Cosmochim. Acta*, *70*(1), 1–12, doi:10.1016/j.gca.2005.08.021.

Affek, H. P., X. Xu, and J. M. Eiler (2007), Seasonal and diurnal variations of $^{13}C^{18}O^{16}O$ in air: Initial observations from Pasadena, CA, *Geochim. Cosmochim. Acta*, *71*, 5033–5043, doi:10.1016/j.gca.2007.08.014.

Aggarwal, P. K., and M. A. Dillon (1998), Stable isotope composition of molecular oxygen in soil gas and groundwater: A potentially robust tracer for diffusion and oxygen consumption processes, *Geochim. Cosmochim. Acta*, *62*(4), 577–584, doi:10.1016/S0016-7037(97)00377-3.

Angert, A., and B. Luz (2001), Fractionation of oxygen isotopes by root respiration: Implications for the isotopic composition of atmospheric O_2, *Geochim. Cosmochim. Acta*, *65*(11), 1695–1701, doi:10.1016/S0016-7037(01)00567-1.

Angert, A., S. Rachmilevitch, E. Barkan, and B. Luz (2003), Effects of photorespiration, the cytochrome pathway, and the alternative pathway on the triple isotopic composition on atmospheric O_2, *Global Biogeochem. Cycles*, *17*(1), 1030, doi:10.1029/2002GB001933.

Appenzeller, C., J. R. Holton, and K. H. Rosenlof (1996), Seasonal variation of mass transport across the tropopause, *J. Geophys. Res.*, *101*(D10), 15,071–15,078, doi:10.1029/96JD00821.

Asprey, L. B. (1976), The preparation of very pure fluorine gas, *J. Fluor. Chem.*, *7*, 359–361, doi:10.1016/S0022-1139(00)84009-9.

Barkan, E., and B. Luz (2005), High precision measurements of $^{17}O/^{16}O$ and $^{18}O/^{16}O$ ratios in H_2O, *Rapid Commun. Mass Spectrom.*, *19*, 3737–3742, doi:10.1002/rcm.2250.

Bender, M. L. (1990), The $\delta^{18}O$ of dissolved O_2 in seawater: A unique tracer of circulation and respiration in the deep sea, *J. Geophys. Res.*, *95*(C12), 22,243–22,252, doi:10.1029/JC095iC12p22243.

Bender, M., T. Sowers, and L. Labeyrie (1994), The Dole effect and its variations during the last 130,000 years as measured in the Vostok ice core, *Global Biogeochem. Cycles*, *8*(3), 363–376, doi:10.1029/94GB00724.

Benedict, M. (1947), Multistage separation processes, *Chem. Eng. Prog.*, *43*(2), 41–60.

Blunier, T., B. Barnett, M. L. Bender, and M. B. Hendricks (2002), Biological oxygen productivity during the last 60,000 years from triple oxygen isotope measurements, *Global Biogeochem. Cycles*, *16*(3), 1029, doi:10.1029/2001GB001460.

Boering, K. A., T. Jackson, K. J. Hoag, A. S. Cole, M. J. Perri, M. Thiemens, and E. Atlas (2004), Observations of the anomalous oxygen isotopic composition of carbon dioxide in the lower stratosphere and the flux of the anomaly to the troposphere, *Geophys. Res. Lett.*, *31*, L03109, doi:10.1029/2003GL018451.

Brasseur, G. P., and S. Solomon (2005), *Aeronomy of the Middle Atmosphere*, Springer, Dordrecht, Netherlands.

Brasseur, G., M. H. Hitchman, S. Walters, M. Dymek, E. Falise, and M. Pirre (1990), An interactive chemical dynamic radiative two-dimensional model of the middle atmosphere, *J. Geophys. Res.*, *95*(D5), 5639–5655, doi:10.1029/JD095iD05p05639.

Brewer, L. (1953), The thermodynamic properties of the oxides and their vaporization processes, *Chem. Rev.*, *52*, 1–75, doi:10.1021/cr60161a001.

Cao, X., and Y. Liu (2012), Theoretical estimation of the equilibrium distribution of clumped isotopes in nature, *Geochim. Cosmochim. Acta*, *77*, 292–303, doi:10.1016/j.gca.2011.11.021.

Coplen, T. B. (2011), Guidelines and recommended terms for expression of stable-isotope-ratio and gas-ratio measurement results, *Rapid Commun. Mass Spectrom.*, *25*(17), 2538–2560.

Craig, H., Y. Horibe, and T. Sowers (1988), Gravitational separation of gases and isotopes in polar ice caps, *Science*, *242*, 1675–1678, doi:10.1126/science.242.4886.1675.

Dennis, K. J., H. P. Affek, B. H. Passey, D. P. Schrag, and J. M. Eiler (2011), Defining an absolute reference frame for 'clumped' isotope studies of CO_2, *Geochim. Cosmochim. Acta*, *75*(22), 7117–7131, doi:10.1016/j.gca.2011.09.025.

Eagle, R. A., E. A. Schauble, A. K. Tripati, T. Tütken, R. C. Hulbert, and J. M. Eiler (2010), Body temperatures of modern and extinct species based on ^{13}C-^{18}O bond abundances in apatite, *Proc. Natl. Acad. Sci. U. S. A.*, *107*(23), 10,377–10,382, doi:10.1073/pnas.0911115107.

Efthimiopoulos, I., K. Kunc, S. Karmakar, K. Syassen, M. Hanfland, and G. Vajenine (2010), Structural transformation and vibrational properties of BaO_2 at high pressures, *Phys. Rev. B*, *82*(13), 134125, doi:10.1103/PhysRevB.82.134125.

Eiler, J. M. (2007), "Clumped-isotope" geochemistry—The study of naturally occurring, multiply substituted isotopologues, *Earth Planet. Sci. Lett.*, *262*, 309–327, doi:10.1016/j.epsl.2007.08.020.

Eiler, J. M. (2011), Paleoclimate reconstruction using carbonate clumped isotope thermometry, *Quat. Sci. Rev.*, *30*(25–26), 3575–3588, doi:10.1016/j.quascirev.2011.09.001.

Eiler, J. M., and E. Schauble (2004), $^{18}O^{13}C^{16}O$ in the Earth's atmosphere, *Geochim. Cosmochim. Acta*, *68*(23), 4767–4777, doi:10.1016/j.gca.2004.05.035.

Eisenstadt, D., E. Barkan, B. Luz, and A. Kaplan (2010), Enrichment of oxygen heavy isotopes during photosynthesis in phytoplankton, *Photosynth. Res.*, *103*, 97–103, doi:10.1007/s11120-009-9518-z.

Engel, A., et al. (2009), Age of stratospheric air unchanged within uncertainties over the past 30 years, *Nat. Geosci.*, *2*(1), 28–31, doi:10.1038/ngeo388.

Gao, Y. Q., and R. A. Marcus (2001), Strange and unconventional isotope effects in ozone formation, *Science*, *293*, 259–263, doi:10.1126/science.1058528.

Ghosh, P., J. Adkins, H. Affek, B. Balta, W. Guo, E. A. Schauble, D. Schrag, and J. M. Eiler (2006), ^{13}C-^{18}O bonds in carbonate materials: A new kind of paleothermometer, *Geochim. Cosmochim. Acta*, *70*(6), 1439–1456, doi:10.1016/j.gca.2005.11.014.

Giannozzi, P., et al. (2009), QUANTUM ESPRESSO: A modular and open-source software project for quantum simulations of materials, *J. Phys. Condens. Matter*, *21*(39), 395502, doi:10.1088/0953-8984/21/39/395502.

Gonze, X., et al. (2002), First-principles computation of material properties: The ABINIT software project, *Comput. Mater. Sci.*, *25*(3), 478–492, doi:10.1016/S0927-0256(02)00325-7.

Guy, R. D., J. A. Berry, M. L. Fogel, and T. C. Hoering (1989), Differential fractionation of oxygen isotopes by cyanide-resistant and cyanice-sensitive respiration in plants, *Planta*, *177*, 483–491, doi:10.1007/BF00392616.

Guy, R. D., M. L. Fogel, and J. A. Berry (1993), Photosynthetic fractionation of the stable isotopes of oxygen and carbon, *Plant Physiol.*, *101*, 37–47.

Hathorn, B. C., and R. A. Marcus (1999), An intramolecular theory of the mass-independent isotope effect for ozone. I, *J. Chem. Phys.*, *111*(9), 4087–4100, doi:10.1063/1.480267.

Hathorn, B. C., and R. A. Marcus (2000), An intramolecular theory of the mass-independent isotope effect for ozone. II. Numerical implementation at low pressures using a loose transition state, *J. Chem. Phys.*, *113*(21), 9497–9509, doi:10.1063/1.1321045.

He, B., G. Olack, and A. Colman (2012), Pressure baseline correction and high precision CO_2 clumped-isotope (Δ_{47}) measurements in bellows and micro-volume modes, *Rapid Commun. Mass Spectrom.*, in press.

Heidenreich, J. E., and M. H. Thiemens (1983), A non-mass-dependent isotope effect in the production of ozone from molecular oxygen, *J. Chem. Phys.*, *78*, 892–895, doi:10.1063/1.444791.

Helman, Y., E. Barkan, D. Eisenstadt, B. Luz, and A. Kaplan (2005), Fractionation of the three stable oxygen isotopes by oxygen-producing and oxygen-consuming reactions in photosynthetic organisms, *Plant Physiol.*, *138*(4), 2292–2298, doi:10.1104/pp.105.063768.

Hoag, K. J., C. J. Still, I. Y. Fung, and K. A. Boering (2005), Triple oxygen isotope composition of tropospheric carbon dioxide as a tracer of terrestrial gross carbon fluxes, *Geophys. Res. Lett.*, *32*, L02802, doi:10.1029/2004GL021011.

Hoffmann, G., et al. (2004), A model of the Earth's Dole effect, *Global Biogeochem. Cycles*, *18*, GB1008, doi:10.1029/2003GB002059.

Holton, J. R., P. H. Haynes, M. E. McIntyre, A. R. Douglass, R. B. Rood, and L. Pfister (1995), Stratosphere-troposphere exchange, *Rev. Geophys.*, *33*(4), 403–439, doi:10.1029/95RG02097.

Holzer, M., C. Orbe, and F. W. Primeau (2012), Stratospheric mean residence time and mean age on the tropopause: Connections and implications for observational constraints, *J. Geophys. Res.*, *117*, D12314, doi:10.1029/2012JD017547.

Huber, K. P., and G. Herzberg (1979), *Molecular Spectra and Molecular Structure*, vol. 4, *Constants of Diatomic Molecules*, edited by G. Herzberg, 736 pp., Van Nostrand Reinhold, New York.

Huntington, K. W., et al. (2009), Methods and limitations of 'clumped' CO_2 isotope (Δ_{47}) analysis by gas-source isotope ratio mass spectrometry, *J. Mass Spectrom.*, *44*(9), 1318–1329, doi:10.1002/jms.1614.

Johnston, J. C., and M. H. Thiemens (1997), The isotopic composition of tropospheric ozone in three environments, *J. Geophys. Res.*, *102*(D21), 25,395–25,404, doi:10.1029/97JD02075.

Jorda, J. L., and T. K. Jondo (2001), Barium oxides: Equilibrium and decomposition of BaO_2, *J. Alloys Compd.*, *327*, 167–177, doi:10.1016/S0925-8388(01)01404-9.

Kaye, J. A., and D. F. Strobel (1983), Enhancement of heavy ozone in the Earth's atmosphere?, *J. Geophys. Res.*, *88*(C13), 8447–8452, doi:10.1029/JC088iC13p08447.

Keeling, R. F. (1995), The atmospheric oxygen cycle: The oxygen isotopes of atmospheric CO_2 and O_2 and the O_2/N_2 ratio, *Rev. Geophys.*, *33*, 1253–1262, doi:10.1029/95RG00438.

Kiddon, J., M. L. Bender, J. Orchardo, D. A. Caron, J. C. Goldman, and M. Dennett (1993), Isotopic fractionation of oxygen by respiring marine organisms, *Global Biogeochem. Cycles*, *7*(3), 679–694, doi:10.1029/93GB01444.

Kroopnick, P., and H. Craig (1976), Oxygen isotope fractionation in dissolved oxygen in the deep sea, *Earth Planet. Sci. Lett.*, *32*, 375–388, doi:10.1016/0012-821X(76)90078-9.

Landais, A., G. Dreyfus, E. Capron, V. Masson-Delmotte, M. F. Sanchez-Goni, S. Desprat, G. Hoffmann, J. Jouzel, M. Leuenberger, and S. Johnsen (2010), What drives the millennial and orbital variations of delta $\delta^{18}O_{atm}$?, *Quat. Sci. Rev.*, *29*(1–2), 235–246, doi:10.1016/j.quascirev.2009.07.005.

Lane, G. A., and M. Dole (1956), Fractionation of oxygen isotopes during respiration, *Science*, *123*(3197), 574–576, doi:10.1126/science.123.3197.574.

Lee, E. S., T. K. Birkham, L. I. Wassenaar, and M. J. Hendry (2003), Microbial respiration and diffusive transport of O_2, $^{16}O_2$, and $^{18}O^{16}O$ in unsaturated soils and geologic sediments, *Environ. Sci. Technol.*, *37*(13), 2913–2919, doi:10.1021/es026146a.

Liang, M.-C., F. W. Irion, J. D. Weibel, C. E. Miller, G. A. Blake, and Y. L. Yung (2006), Isotopic composition of stratospheric ozone, *J. Geophys. Res.*, *111*, D02302, doi:10.1029/2005JD006342.

Liang, M.-C., G. A. Blake, B. R. Lewis, and Y. L. Yung (2007), Oxygen isotopic composition of carbon dioxide in the middle atmosphere, *Proc. Natl. Acad. Sci. U. S. A.*, *104*(1), 21–25, doi:10.1073/pnas.0610009104.

Luz, B., and E. Barkan (2011), The isotopic composition of atmospheric oxygen, *Global Biogeochem. Cycles*, *25*, GB3001, doi:10.1029/2010GB003883.

Luz, B., E. Barkan, M. L. Bender, M. H. Thiemens, and K. A. Boering (1999), Triple-isotope composition of atmospheric oxygen as a tracer of biosphere productivity, *Nature*, *400*(6744), 547–550, doi:10.1038/22987.

Martinerie, P., G. P. Brasseur, and C. Granier (1995), The chemical composition of ancient atmospheres: A model study constrained by ice core data, *J. Geophys. Res.*, *100*(D7), 14,291–14,304, doi:10.1029/95JD00826.

Mauersberger, K., B. Erbacher, D. Krankowsky, J. Günther, and R. Nickel (1999), Ozone isotope enrichment: Isotopomer-specific rate coefficients, *Science*, *283*, 370–372, doi:10.1126/science.283.5400.370.

Miller, M. F. (2002), Isotopic fractionation and the quantification of ^{17}O anomalies in the oxygen three-isotope system: An appraisal and geochemical significance, *Geochim. Cosmochim. Acta*, *66*(11), 1881–1889, doi:10.1016/S0016-7037(02)00832-3.

Morton, J., J. Barnes, B. Schueler, and K. Mauersberger (1990), Laboratory studies of heavy ozone, *J. Geophys. Res.*, *95*(D1), 901–907, doi:10.1029/JD095iD01p00901.

Naylor, R. W., and P. O. Backer (1955), Enrichment calculations in gaseous diffusion: Large separation factor, *AIChE J.*, *1*(1), 95–99, doi:10.1002/aic.690010114.

Perdew, J. P., K. Burke, and M. Ernzerhof (1996), Generalized gradient approximation made simple, *Phys. Rev. Lett.*, *77*(18), 3865–3868, doi:10.1103/PhysRevLett.77.3865.

Plumb, R. A. (2007), Tracer interrelationships in the stratosphere, *Rev. Geophys.*, *45*, RG4005, doi:10.1029/2005RG000179.

Rappe, A. M., K. M. Rabe, E. Kaxiras, and J. D. Joannopoulos (1990), Optimized pseudopotentials, *Phys. Rev. B*, *41*(2), 1227–1230, doi:10.1103/PhysRevB.41.1227.

Rind, D., J. Lerner, C. McLinden, and J. Perlwitz (2009), Stratospheric ozone during the Last Glacial Maximum, *Geophys. Res. Lett.*, *36*, L09712, doi:10.1029/2009GL037617.

Rosenlof, K. H. (1995), Seasonal cycle of the residual mean meridional circulation in the stratosphere, *J. Geophys. Res.*, *100*(D3), 5173–5191, doi:10.1029/94JD03122.

Schauble, E. A., P. Ghosh, and J. M. Eiler (2006), Preferential formation of ^{13}C-^{18}O bonds in carbonate minerals, estimated using first-principles lattice dynamics, *Geochim. Cosmochim. Acta*, *70*(10), 2510–2529, doi:10.1016/j.gca.2006.02.011.

Severinghaus, J. P., and M. O. Battle (2006), Fractionation of gases in polar ice during bubble close-off: New constraints from firn air Ne, Kr and Xe observations, *Earth Planet. Sci. Lett.*, *244*, 474–500, doi:10.1016/j.epsl.2006.01.032.

Severinghaus, J. P., M. L. Bender, R. F. Keeling, and W. S. Broecker (1996), Fractionation of soil gases by diffusion of water vapor, gravitational settling, and thermal diffusion, *Geochim. Cosmochim. Acta*, *60*(6), 1005–1018, doi:10.1016/0016-7037(96)00011-7.

Severinghaus, J. P., R. Beaudette, M. A. Headly, K. Taylor, and E. J. Brook (2009), Oxygen-18 of O_2 records the impact of abrupt climate change on the terrestrial biosphere, *Science*, *324*(5933), 1431–1434, doi:10.1126/science.1169473.

Starokon, E. V., M. V. Parfenov, S. E. Malykhin, and G. I. Panov (2011), Catalytic role of O^- radicals in the low-temperature isotopic exchange in dioxygen, *J. Phys. Chem. C*, *115*(25), 12,554–12,559, doi:10.1021/jp203022s.

Thiemens, M. H., and D. Meagher (1984), Cryogenic separation of nitrogen and oxygen in air for determination of isotopic ratios by mass spectrometry, *Anal. Chem.*, *56*(2), 201–203, doi:10.1021/ac00266a018.

Thiemens, M. H., T. Jackson, E. C. Zipf, P. W. Erdman, and C. van Egmond (1995), Carbon dioxide and oxygen isotope anomalies in the mesosphere and stratosphere, *Science*, *270*(5238), 969–972, doi:10.1126/science.270.5238.969.

Thompson, A. M. (1992), The oxidizing capacity of the Earth's atmosphere: Probable past and future changes, *Science*, *256*(5060), 1157–1165, doi:10.1126/science.256.5060.1157.

Tribelhorn, M. J., and M. E. Brown (1995), Thermal decomposition of barium and strontium peroxides, *Thermochim. Acta*, *255*, 143–154, doi:10.1016/0040-6031(94)02156-I.

Vanderbilt, D. (1990), Soft self-consistent pseudopotentials in a generalized eigenvalue formalism, *Phys. Rev. B*, *41*(11), 7892–7895, doi:10.1103/PhysRevB.41.7892.

Van Wyngarden, A. L., K. A. Mar, K. A. Boering, J. J. Lin, Y. T. Lee, S.-Y. Lin, H. Guo, and G. Lendvay (2007), Nonstatistical behavior of reactive scattering in the $^{18}O + {}^{32}O_2$ isotope exchange reaction, *J. Am. Chem. Soc.*, *129*(10), 2866–2870, doi:10.1021/ja0668163.

Vinnikov, K. Y., and N. C. Grody (2003), Global warming trend of mean tropospheric temperature observed by satellites, *Science*, *302*(5643), 269–272, doi:10.1126/science.1087910.

Wahlbeck, P. G. (1971), Effusion. VII. The failure of isotropy of a gas in an effusion cell and the transition region, *J. Chem. Phys.*, *55*(4), 1709–1715, doi:10.1063/1.1676300.

Wang, Z., E. A. Schauble, and J. M. Eiler (2004), Equilibrium thermodynamics of multiply substituted isotopologues of molecular gases, *Geochim. Cosmochim. Acta*, *68*(23), 4779–4797, doi:10.1016/j.gca.2004.05.039.

Wiegell, M. R., N. W. Larsen, T. Pedersen, and H. Egsdard (1997), The temperature dependence of the exchange reaction between oxygen atoms and dioxygen molecules studied by means of isotopes and spectroscopy, *Int. J. Chem. Kinet.*, *29*(10), 745–753, doi:10.1002/(SICI)1097-4601(1997)29:10<745::AID-KIN3>3.0.CO;2-M.

Yeung, L. Y., H. P. Affek, K. J. Hoag, W. Guo, A. A. Wiegel, E. L. Atlas, S. M. Schauffler, M. Okumura, K. A. Boering, and J. M. Eiler (2009), Large and unexpected enrichment in stratospheric $^{16}O^{13}C^{18}O$ and its meridional variation, *Proc. Natl. Acad. Sci. U. S. A.*, *106*(28), 11,496–11,501, doi:10.1073/pnas.0902930106.

Young, E. D., A. Galy, and H. Nagahara (2002), Kinetic and equilibrium mass-dependent isotope fractionation laws in nature and their geochemical and cosmochemical significance, *Geochim. Cosmochim. Acta*, *66*(6), 1095–1104, doi:10.1016/S0016-7037(01)00832-8.

Yung, Y. L., W. B. DeMore, and J. P. Pinto (1991), Isotopic exchange between carbon dioxide and ozone via $O(^1D)$ in the stratosphere, *Geophys. Res. Lett.*, *18*(1), 13–16, doi:10.1029/90GL02478.

Yung, Y. L., A. Y. T. Lee, F. W. Irion, W. B. DeMore, and J. Wen (1997), Carbon dioxide in the atmosphere: Isotopic exchange with ozone and its use as a tracer in the middle atmosphere, *J. Geophys. Res.*, *102*(D9), 10,857–10,866, doi:10.1029/97JD00528.